Supporting information

In vitro Studies on the Selective Cytotoxic Effect of Luminescent Ru(II)-*p*-Cymene Complexes of Imidazo-Pyridine and Imidazo Quinoline Ligands

Pravinkumar Selvam[a†], Sourav De[a,d†], Priyankar Paira[a], S. K. Ashok Kumar[a*], Selva Kumar R[b], Anbalagan Moorthy[c], Arjita Ghosh[c], Yung-Chih Kuo[d], Subhasis Banerjee[e], Shantha Kumar Jenifer[f]

[a]Department of Chemistry, School of Advanced Sciences, Vellore Institute of Technology, Vellore-632014, Tamil Nadu, India. E-mail: ashokkumar.sk@vit.ac.in

[b]Department of Chemistry, Saveetha School of Engineering, Saveetha Institute of Medical and Technical Science (SIMATS), Chennai – 602105, Tamil Nadu, India.

[c]Department of Biotechnology, School of Bioscience & Technology, Vellore Institute of Technology, Vellore 632014, Tamil Nadu, India

[d]Department of Chemical Engineering, National Chung Cheng University, Chia-Yi, Taiwan 62102, ROC

[e]Department of Pharmaceutical Chemistry, Gupta College of Technological Sciences. Asansol-713301, West Bengal. India

[f] DST Unit of Nanoscience (DST UNS) and Thematic Unit of Excellence (TUE), Department of Chemistry, Indian Institute of Technology Madras, Chennai - 600 036, India

†Authors care contributed equally.

Contents

Experimental Procedure

Figures

Tables

Experimental Procedure

1. UV-Vis and Fluorescence Study

The spectral response of UV-Visible and fluorescence studies of **L_1**, **L_2**, **Ru-1** and **Ru-2** were conducted in 10% DMSO solution. Fluorescence quantum yield (φ) was estimated by using the comparative William's method in water and MTT media [1]. Tryptophan was used as a reference compound (0.16 in 0.1 M NaOH), excited at 275 nm and emission was recorded at 353 nm. Both absorption and emission spectra of reference and lead compound (3×10^{-5} M) were used. The gradients of the plots are proportional to the quantum yield (φ) of the studied system. The quantum yield value was calculated according to the equation (i):

$$\varphi = \varphi_R \times \frac{I_S}{I_R} \times \frac{OD_R}{OD_S} \times \frac{\eta_S}{\eta_R} \qquad (i)$$

Where, φ, I, OD and η related to quantum yield, peak area, absorbance at $\lambda_{max,}$ refractive index of solvent.

2. Stability Study

The stability of **L_1**, **L_2**, **Ru-1** and **Ru-2** were established in water, MTT and GSH medium.

3. Electrolytic Study

To know the ionic nature of the lead compound, molar conductivity of ligand and Ru(II) complexes were performed in water, DMSO and DMF media. The molar conductivity of each solution was measured using a conductivity-TDS meter-307 (Systronics, India) with cell constant 1.0 cm^{-1} [2] and Λ_M was calculated using the formula (ii).

$$\Lambda_M = \frac{K \times 1000}{C} \qquad (ii)$$

Where, K= specific conductivity and C= concentration of solute.

4. DNA Binding Study

4.1 Electronic Absorption Spectra

The DNA binding experiment was performed with **L_1**, **L_2**, **Ru-1** and **Ru-2** (3×10^{-5} M) in Tris-HCl buffer (pH 7.4) in water medium [3]. The concentration of CT-DNA was calculated spectrophotometrically at 260 nm using its molar absorption coefficient value 6600 L. M^{-1} cm^{-1}. Primarily, an equivalent amount of DNA (1 mL, 2.87×10^{-4} M) was added to both cuvettes (sample and reference) and chronologically added ligands to get absorption spectra of DNA-ligand interaction. Initially, lead compound was equilibrated with CT-DNA for about 5 min. The intrinsic DNA binding constant (K_b) was calculated using the equation (iii). Also, the UV-visible absorbance spectra of ligand were taken in aqueous medium.

$$\frac{DNA}{(\varepsilon_{a\_} \varepsilon_f)} = \frac{DNA}{(\varepsilon_b - \varepsilon_f)} + \frac{1}{K_b(\varepsilon_a - \varepsilon_f)} \qquad (iii)$$

Where ε_a, ε_f and ε_b are the apparent extinction coefficient for the complex, extinction coefficient of the complex in its free form and extinction coefficient of the complex when fully bound to DNA respectively [4]. The linear plot has been made by plotting [DNA]/(ε_a-ε_f) vs. [DNA] using Origin Lab, version 8.5. The K_b value of lead compound was calculated from the ratio of the slope and intercept.

4.2 Relative Viscosity Study

Viscosity study has been performed to find out the mode of binding interaction of complex with DNA using Ostwald's capillary viscometer [5-7]. Each experiment was executed for three times, and the average flow time was documented. The data was plotted as $(\eta/\eta_0)^{1/3}$ vs. [complex]/[DNA], where η and η_0 relates to viscosity of DNA in the presence and absence of the ligand respectively. The viscosity of DNA was calculated using the formula (iv), where t and t_0 signifies the efflux time of DNA and PBS buffer solution respectively.

$$\eta_0 = \frac{(t - t_0)}{t_0} \qquad (iv)$$

4.3 EtBr Displacement Assay

The competitive binding was performed to know the mechanism of binding between the lead compounds with DNA-bound EtBr [8]. Upon interacting EtBr with DNA, an intense fluorescence emission is taken place owing to the formation of the EtBr-DNA adduct. Under such environment upon adding lead compound to this environment, the lead compound

undergo intercalation in DNA and subsequently, it displaces EtBr from DNA, due to this there is reduction in fluorescence. The apparent binding constant of the ligand to CT-DNA was calculated from the measurements of fluorescence intensity. EtBr exhibits weak fluorescence in Tris-buffer owing to quenching of free EtBr by solvent molecules. But in presence of DNA, emission intensity dramatically enhanced because of its intercalative binding affinity which revealed that substantial decrease fluorescence intensity. The interaction tendency of the lead compound with DNA was measured from the fall in emission intensity. The K_{app} data obtained from the following equation (v)

$$K_{app} \times [complex]_{50} = K_{EtBr} \times [EtBr] \qquad (v)$$

where $[complex]_{50}$ signifies the concentration of the complex at 50% quenching of DNA-bound EtBr emission intensity, K_{EtBr}=1.0 × 10^7 M^{-1}, binding constant of EtBr and concentration of EtBr is used 8 μM. K_{SV} is Stern-Volmer quenching constant [9]. The value of K_{SV} was calculated using equation (vi).

$$\frac{I_0}{I} = 1 + K_{SV}[Q] \qquad (vi)$$

Where I_0 and I are emission intensities of EtBr-DNA in the absence and presence of compound of concentration [Q].

4.4 DNA Cleaving Study

Agarose gel electrophoresis techniques are used to find out the ability of lead compound to damage the DNA double helix. In the beginning, approximately 200 ng of plasmid DNA (~1 kb) was mixed in 1mL of PBS buffer solution. Later, equal amount of variable concentration of ligand was added into the mixture and the solution was incubated for about 1h at 37^0 C. The mixture was mixed DNA loading dye (bromophenol blue (25%), xylene cyanol (0.25%), and glycerol (30%) and loaded on 1% agarose gel containing EtBr (1.0 mg/ml). Here plasmid DNA incubated without any compound was used as control. Electrophoresis was carried out at 50V for 2 h. At last, the gel image was taken by using Bio-Rad GelDoc instrument [10].

5. Protein Binding Study

5.1 Emission study

In order to calculate the binding interaction between the lead compounds and protein, fluorescence emission technique has been used [11]. In order to investigate the effect of lead compounds with BSA, the fluorescence spectra were performed in Tris-HCl/NaCl buffer (TBS, pH 7.4). Initially, 66 mg of BSA was taken in a 2 mL eppendorf and 1 mL of Tris-HCl/NaCl buffer was added followed calculate the concentration of the BSA protein. The resulting stock concentration is 1 × 10^{-3} M, simultaneously, ligand solution was made to carry out the titration progress. Firstly, 2 mL of buffer transferred to cuvette which contain BSA protein (2 × 10^{-5} M) and sequentially increasing the concentration of ligand to get decrease emission spectra which revealed that BSA-ligand interaction. Before each measurement, sample was equilibrated with BSA for about 5 min. The quenching of the emission at 340 nm (λ_{ex}, 295 nm) was recorded. The quenching constant (K_{BSA}) was calculated by using Stern-Volmer equation (vii).

$$\frac{I_0}{I} = 1 + K_{BSA}[Q] = 1 + K_q\tau_0[Q] \qquad (vii)$$

$$K_q = \frac{K_{BSA}}{\tau_0} \qquad (viii)$$

$$log\frac{I_0 - I}{I} = \log K + nlog[Q] \qquad (ix)$$

Where, I_0 and I are fluorescence intensities of BSA in the absence and presence of quencher of concentration [Q] while K_{SV}, k_q and τ_0 are related to quenching constant, quenching rate constant and average lifetime of the tryptophan (1×10^{-8} s), while K and n signifies binding constant and number of binding sites calculated by using Scatchard equation (ix) [12].

5.2 Isothermal titration calorimetry (ITC)

ITC experiments have been executed to find out the interaction of the complexes **Ru-1** (0.09 M) and **Ru-2** (0.09 M) with BSA (0.009 M) and CT-DNA (0.009M) in DMSO:water (0.5:9.5,v/v) at 23°C using the MicroCal iTC200 system. The instrument consists of a reference cell that has heat capacity like the sample cell solution. The reference cell was filled with water. The sample cell before being used for experiment was thoroughly washed with DMSO:water (0.5:9.5,v/v). The sample cell was loaded with BSA in which the heat released by dilution of BSA in the cell is negligible. **Ru-I** (0.09M) or **Ru-2** (0.09M) was loaded into the 40 µL syringe

and titrated with BSA (0.009M) solution. More Ru(II) complex solution is added and process repeated until no differences in heat are recorded and the area under curves integrated to yield heat transferred. A similar experiment was carried out using Ru(II) complex (0.09 M) with CT-DNA (0.009M) solution. Titration was performed by using the automated syringe filled with the Ru(II)-complex solution with continuous stirring at 500 rpm throughout the experiments. Injections were initiated (1 µL) after baseline stability was established. A titration experiment consisted of 30 consecutive injections of 5 µL volume and 10 min duration each, with a filter period of 10 s. The reference power was set at 10 µcal/s with an initial delay of 60 s. Control experiments were performed by titrating Ru(II) complex into a 5% aqueous DMSO media to ignore the contribution of solvent media interaction. The resulting data were fitted by a sequential binding site model using MicroCal ORIGIN software supplied with the instrument to give stoichiometry (N), binding constant (Ka) enthalpy change (ΔH) and entropy change (ΔS). The change in free energy was calculated using Gibb's free energy equation (ΔG= ΔH-TΔS) [13].

7. *In-Vitro* Cytotoxicity

It is based on the reduction of the yellow tetrazolium salt (3-[4, 5-dimethyl thiazol-2-yl]-2, 5 diphenyl tetrazolium bromide) by mitochondrial dehydrogenases to form a blue MTT formazan in viable cells [14-17]. Each compound was dissolved in 0.1% DMSO and then serial diluted with DMEM medium containing 10% Fetal calf serum. Different cell lines such as HeLa, MCF-7, MDA-MB-231 and HEK-293 were used in this assay. The *cis*platin was used as a positive control. The entire cells were cultured in 100 µL of a growth medium in 96-well plates and incubated at 37°C under 5% CO_2 overnight. After incubation time, the cultured cells were exposed to different concentrations of compounds (9-300 µM). Control cells cultured with an equivalent amount of DMSO alone. After 24 h of incubation time, 100 µL of MTT reagent (1 mg/mL) was added in each culture wells and incubated for 3 h at 37°C. After 3 h, the medium was discarded and formazan crystals formed in live cells were dissolved in 300 µl DMSO and subsequently quantitated by measuring absorbance using ELISA reader at 620 nm. The experiment was also conducted in triplicate. The growth inhibition percentage was calculated using the formula: percentage growth inhibition = 100-[(AD×100)/AB], where AD represents measured absorbance in wells which consists samples and AB represents absorbance of the blank wells.

8. Octanol water partition coefficients

The log P of lead compound was determined *via* the conventional shake-flask method [18]. A fixed amount of lead compound was suspended in water (pre-saturated with n-octanol) and shaken for 48 h on an orbital shaker. To allow phase separation, the solution was centrifuged for 10 min at 3000 rpm. Then the amount of lead compound present in the saturated aqueous solution was measured by UV-Visible spectrophotometer.

9. Drug-likeness Studies

All the compounds were checked for their drug likeness by generating data pertaining to molecular weight, number of hydrogen bond donors/acceptors, polar surface area, number of rotatable bonds, partition coefficient, etc. The study was carried out using an online web-server named Swiss ADME (Molecular modelling group, Swiss Institute of Bioinformatics, Lausanne, Switzerland) [19].

10. ADME Profiling

Absorption, Distribution, Metabolism, Excretion (ADME) prediction study helps in developing safest drug in a faster manner. In the current study, as a part of secondary screening, this ADME profiling was conducted [20].

11. Molecular Docking and Quantum Computational

The lead molecules were exposed to molecular docking study using Autodock vina [21], covering Lamarckian genetic algorithm (LGA) to calculate binding affinities of several conformers and AutoDock Tools (ADT) to implement the operation and consequent calculations. With the current computational resources, such a huge docking calculation with the large experimental HS-DNA prompted the process to opt a smaller section of DNA with the sequence d(CCGTCGACGG) (PDB entry: 423D, a sequence commonly used in oligodeoxynucleotide study) [22] obtained from Protein Data Bank [23] with resolution of 1.60 Å was built using Autodock4 package to expedite over DNA-binding properties of all the ligands and their respective Ru-complexes considered for the present study. The 2D structures of (**L_1**, **L_2**, **Ru-1**, and **Ru-2**) drawn using ACD ChemSketch Freeware, from which all the corresponding coordinates were obtained and subsequently transformed into PDB form through a toolbox that can speak several languages of chemical data [24]. Separate files for

both DNA and lead molecules were made using AutoDock Tools. Each atom in both target and lead compound was fed with Gasteiger charges. Prior docking, the binding site was assigned developing a grid box with a spacing of 1 Å and 26 × 26 × 26 number of points was used in x, y and z directions. The target was further developed to pdbqt for the final operation. With an exhaustiveness of 8, Autodock generated nine significant conformers for each ligand and their respective Ru-complexes. The necessary calculations were done in a Dell system (3.4 GHz processor, 4GB RAM, 1 TB Hard disk operating system). The scoring functions obtained out of the process were screened to fix the conformer lying close to the active site residues and subsequently analysed for its binding pattern. PyMOL (The PyMOL Molecular Graphics System, Version 1.3, Schrodinger, LLC) molecular graphics program was used to study the orientation of each conformer within the active site.

In order to rationalize the experimental protein binding study, molecular docking study was performed. The crystallographic structure of BSA with the PDB ID: 4F5S [25] was collected from fetched from the protein data bank. The additional thing done during the protein preparation was the exclusion of water molecule in order to avoid the unwanted interaction with the docked conformers. The grid size considered for the protein is 30, 26 and 24 along the X, Y and Z axes with a spacing of 1 Å encircling all the putative active site residues of which the most prominent are Trp213 and Trp134 [26]. The working principle and the output parameters were as similar as the above-mentioned DNA docking.

The DFT (density functional theory) analysis of lead molecules was performed using Gaussian 09 and visualized through Gauss view 6.0. The structural coordinates of the lead compounds were optimized using B3LYP/6–31 G (d,p) level basis set without any symmetrical constraints [27]. The standard basis set 6-311G (d,p) was assigned for lighter elements such as C, H, N, Cl and LanL2DZ effective core potential for Ru atom [28]. All geometry has been optimized to zero negative vibration frequency represent the local minima associated with positive Eigen values. Vertical electronic excitations based on B3LYP will be obtained with the time-dependent density functional theory (TD-DFT) theory in the gas phase using the ground state optimized geometry [29].

Spectral Data

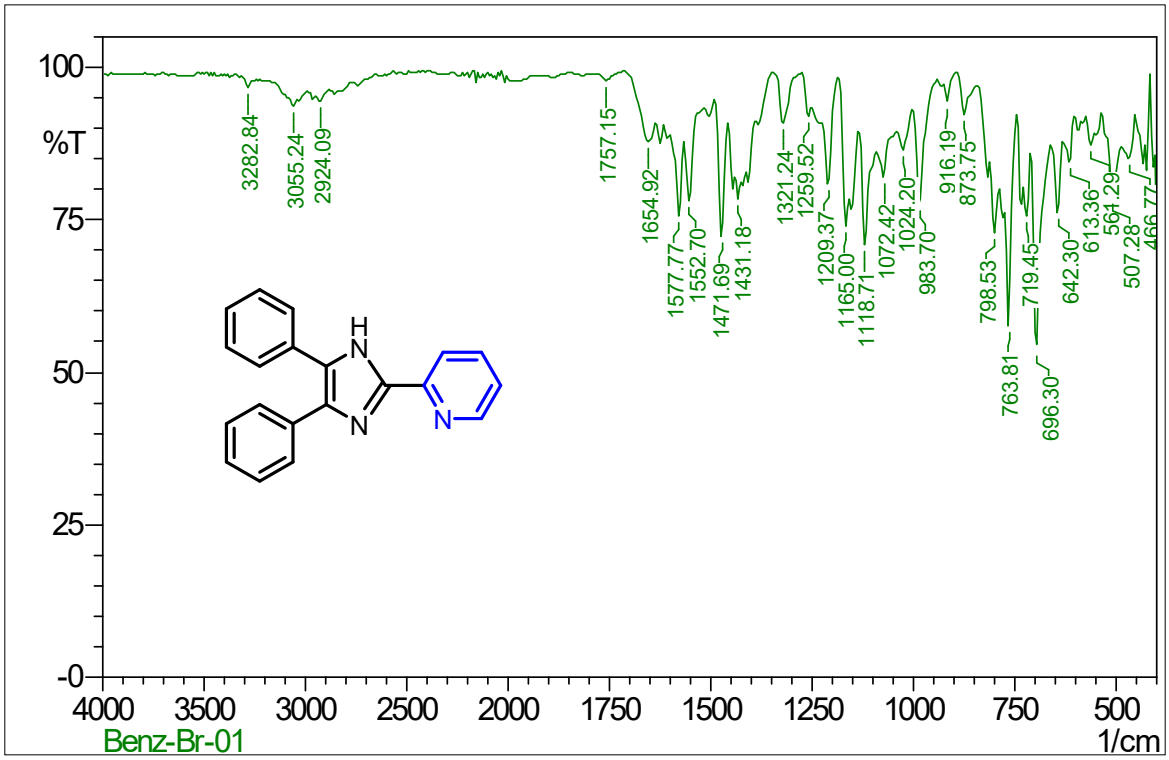

Fig. S1 FTIR spectrum of L_1

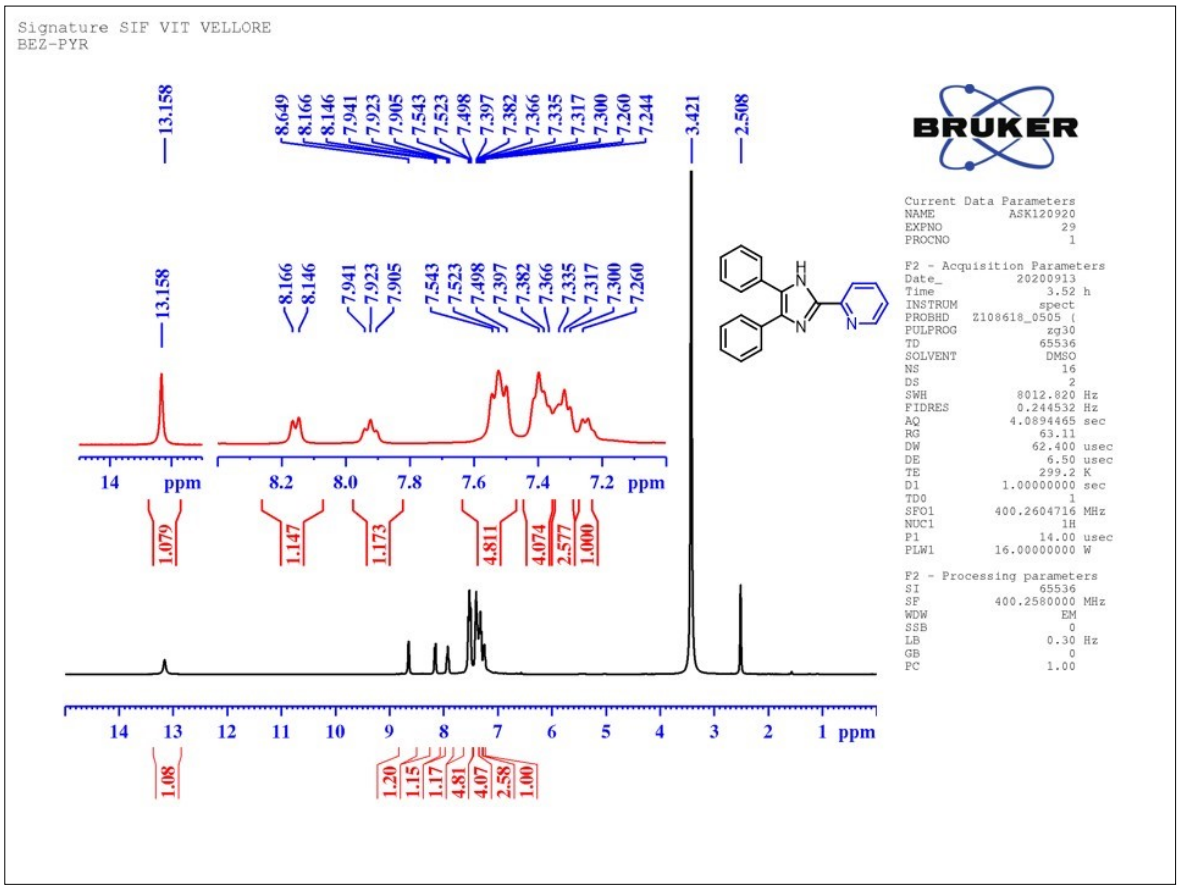

Fig. S2 ^{1}H NMR spectrum of $\mathbf{L_1}$

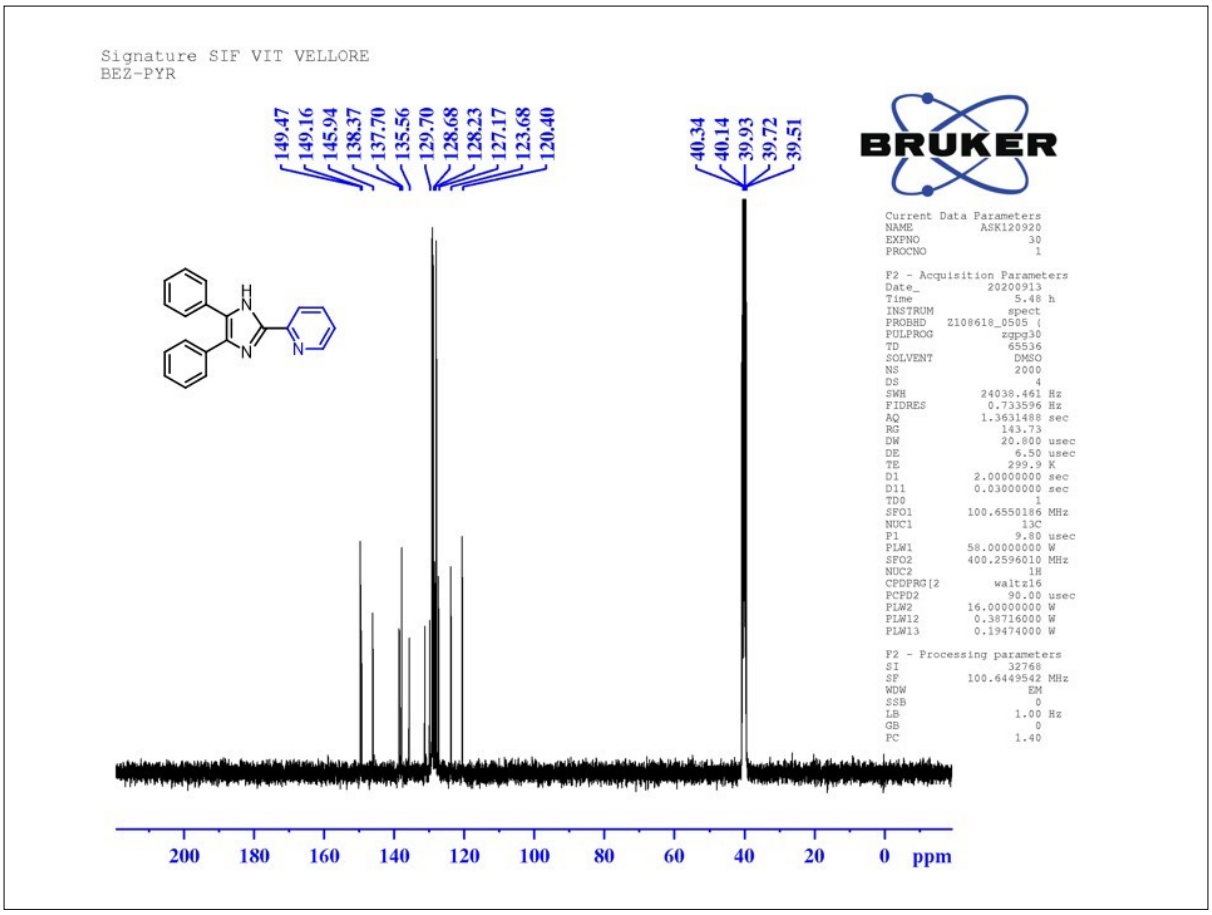

Fig. S3 ^{13}C NMR spectrum of $\mathbf{L_1}$

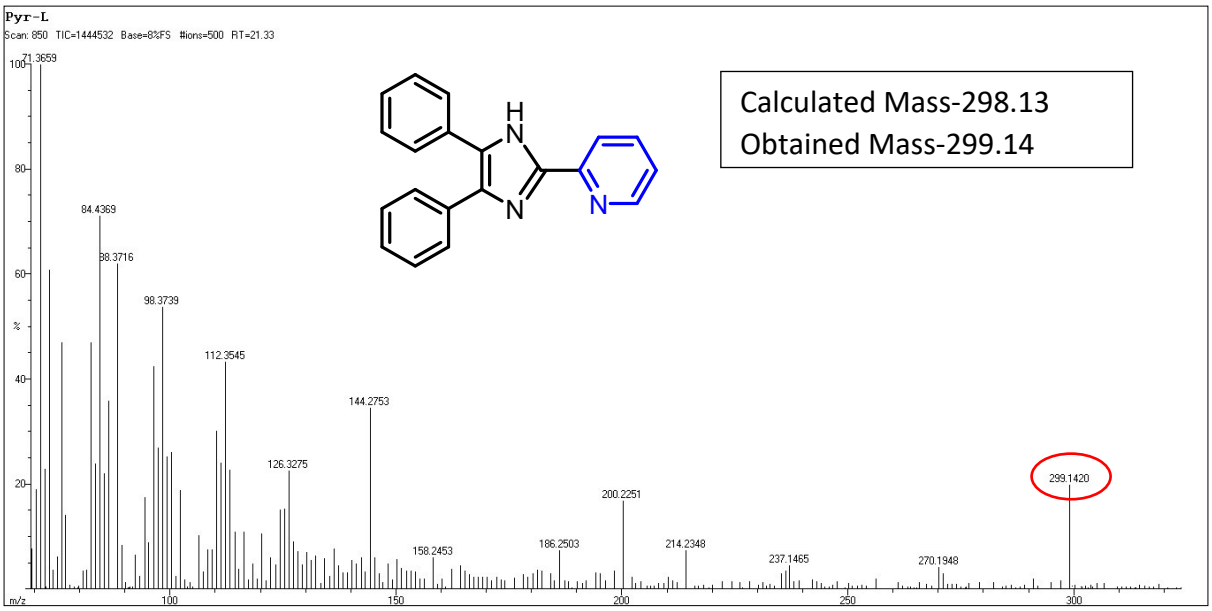

Fig. S4 HR-MS spectrum of $\mathbf{L_1}$

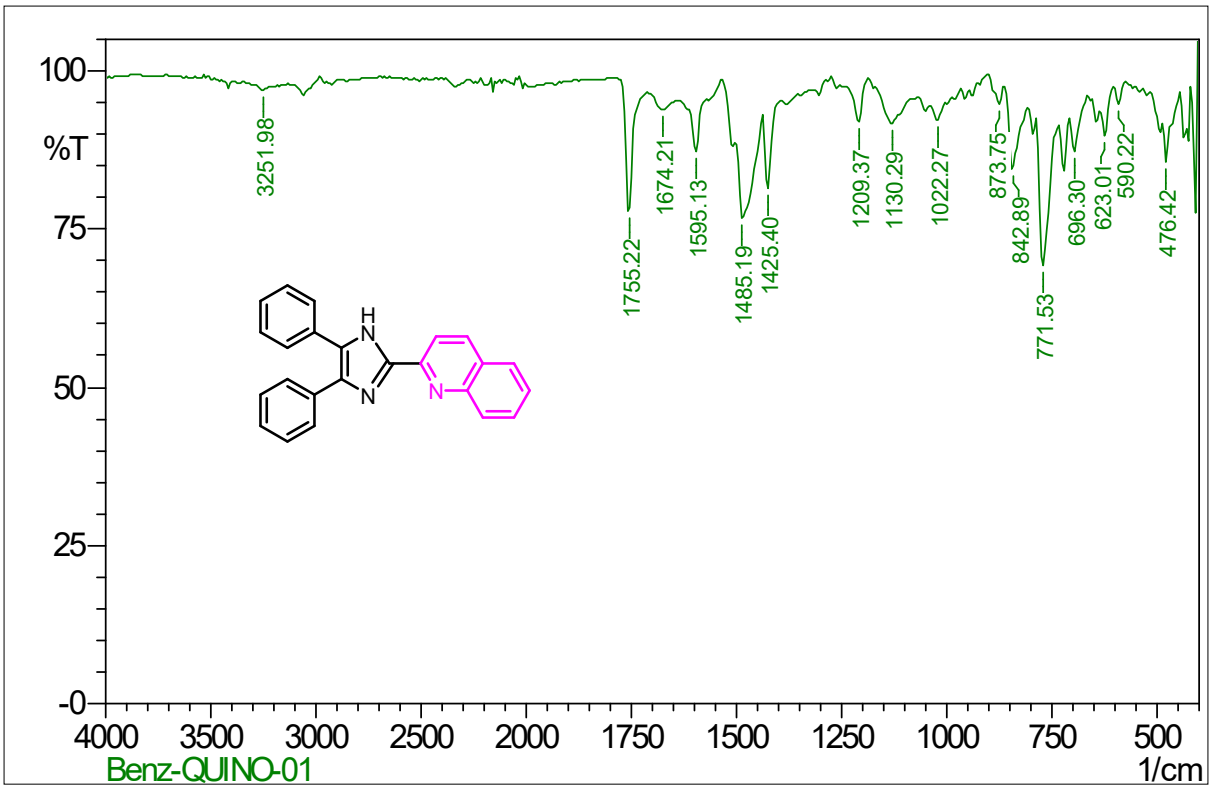

Fig. S5 FTIR spectrum of L_2

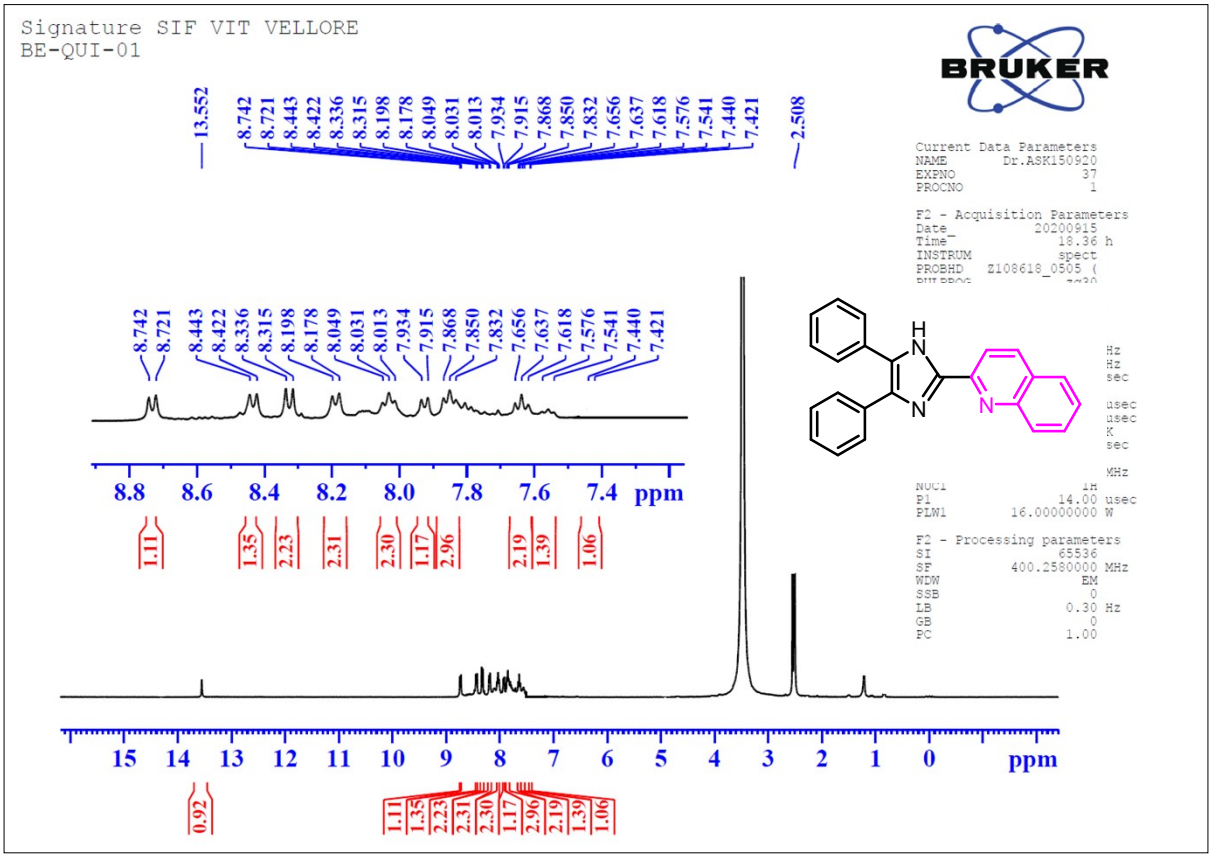

Fig. S6 ^{1}H NMR spectrum of L_2

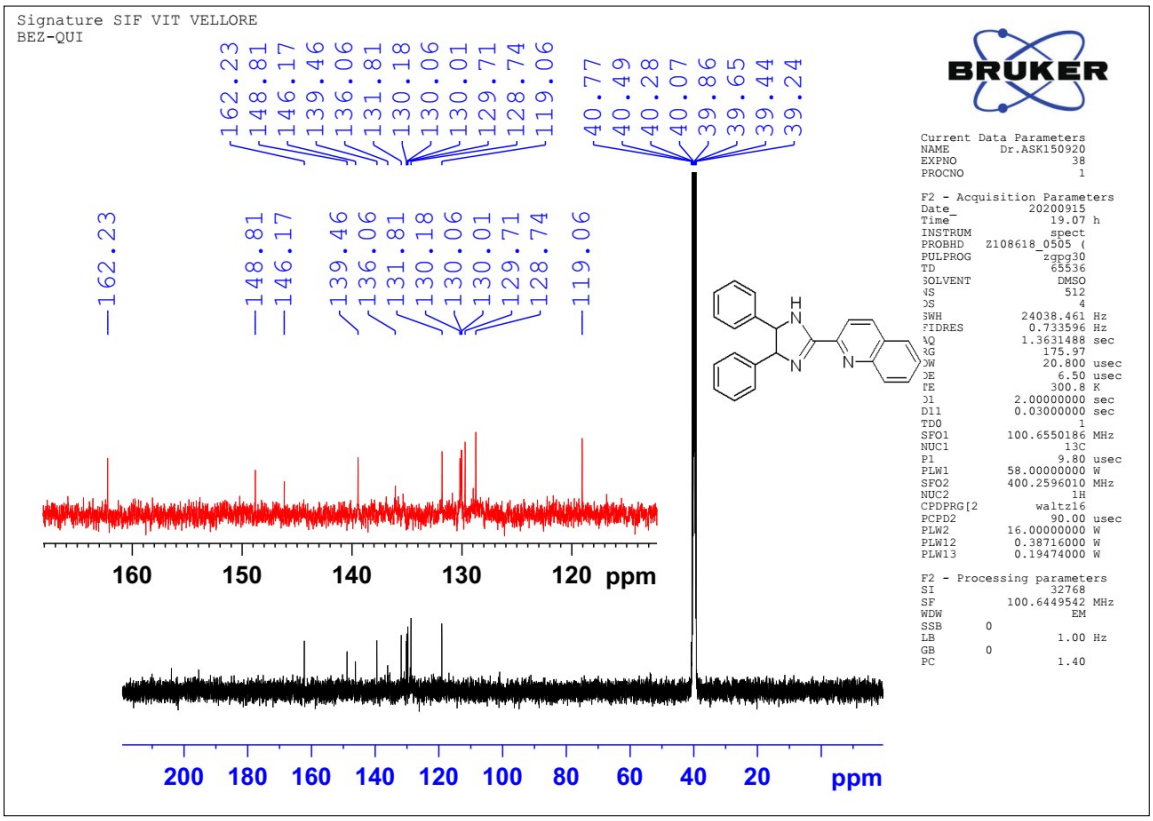

Fig. S7 ^{13}C NMR spectrum of **L_2**

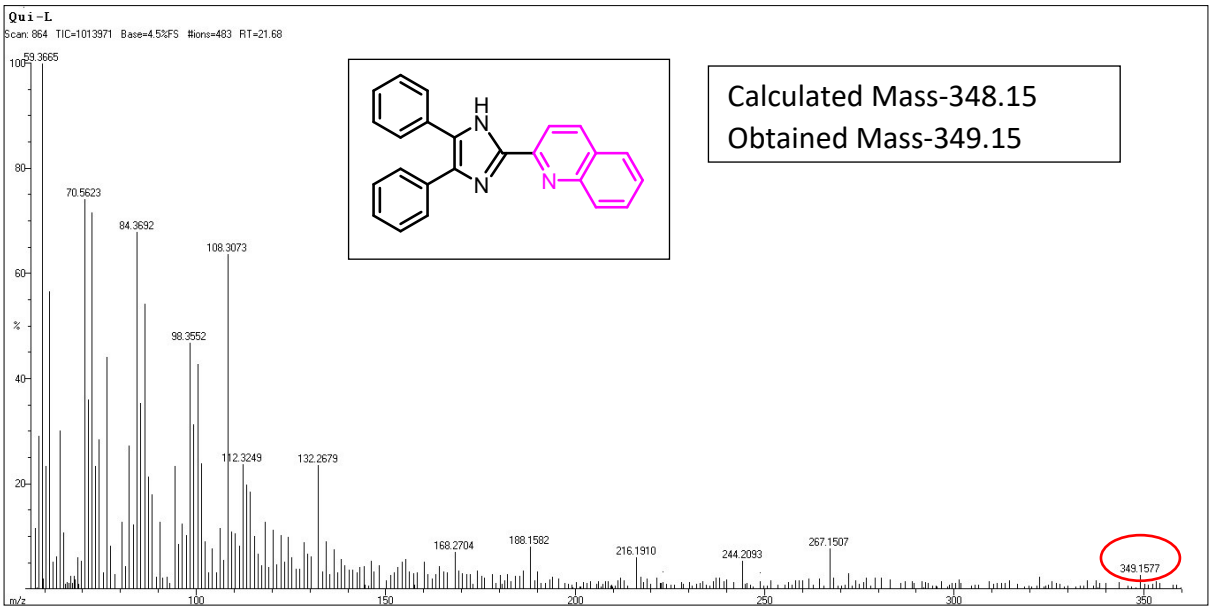

Fig. S8 HR-MS spectrum of **L_2**

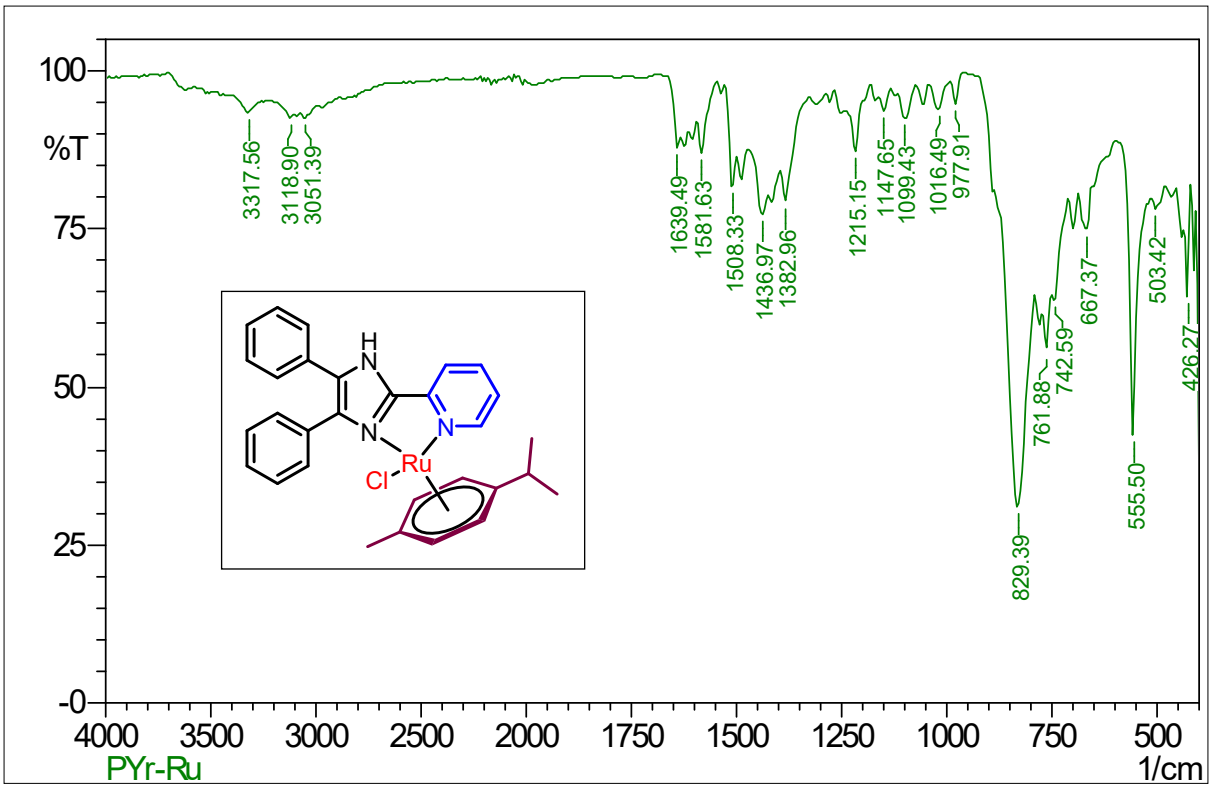

Fig. S9 FTIR spectrum of **Ru-1**

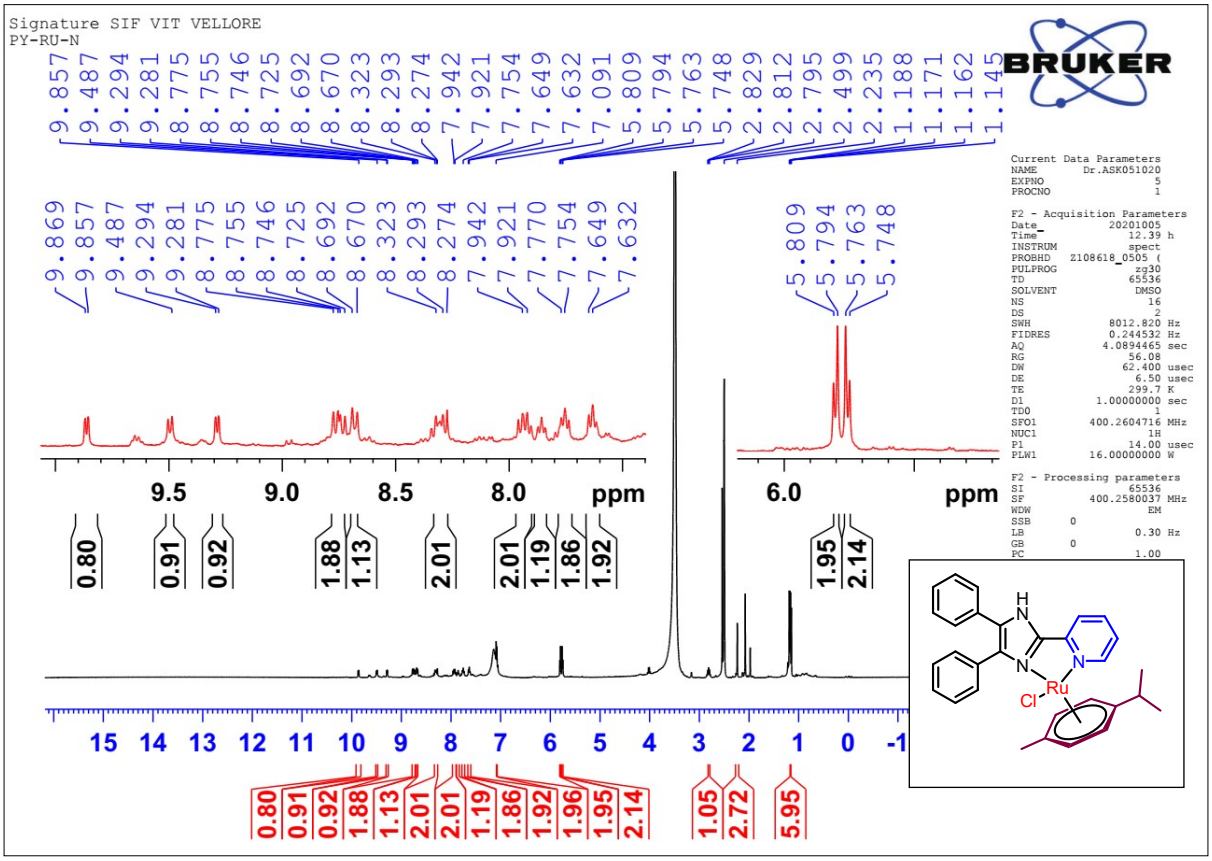

Fig. S10 ^{1}H NMR spectrum of **Ru-1**

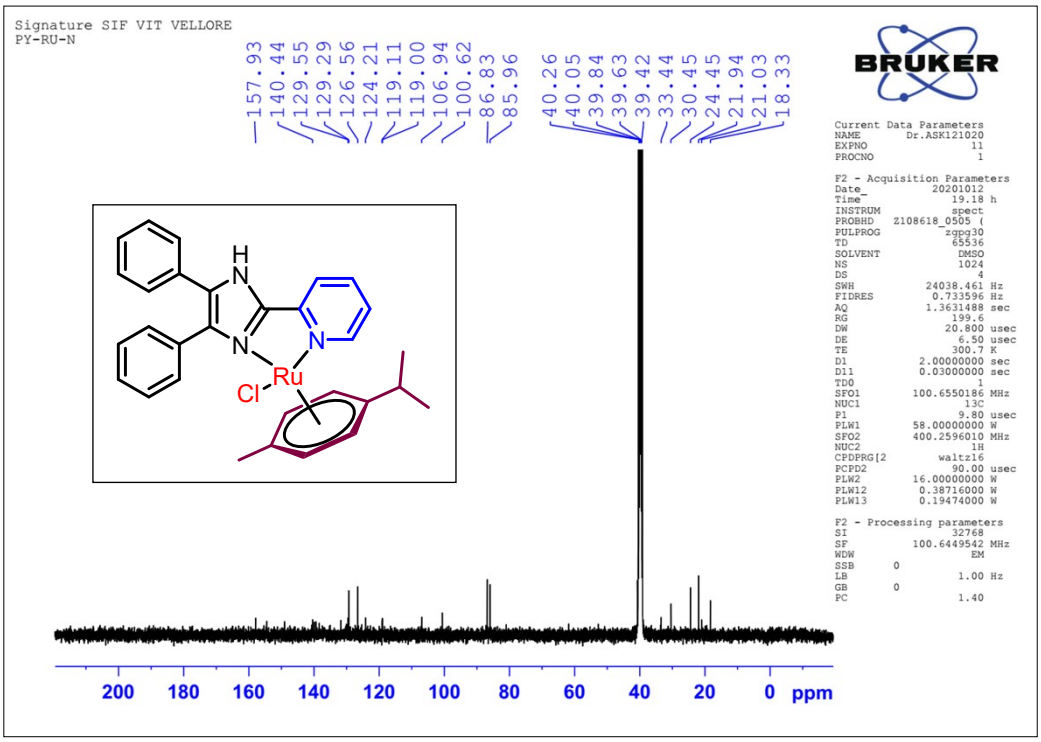

Fig. S11 ^{13}C NMR spectrum of **Ru-1**

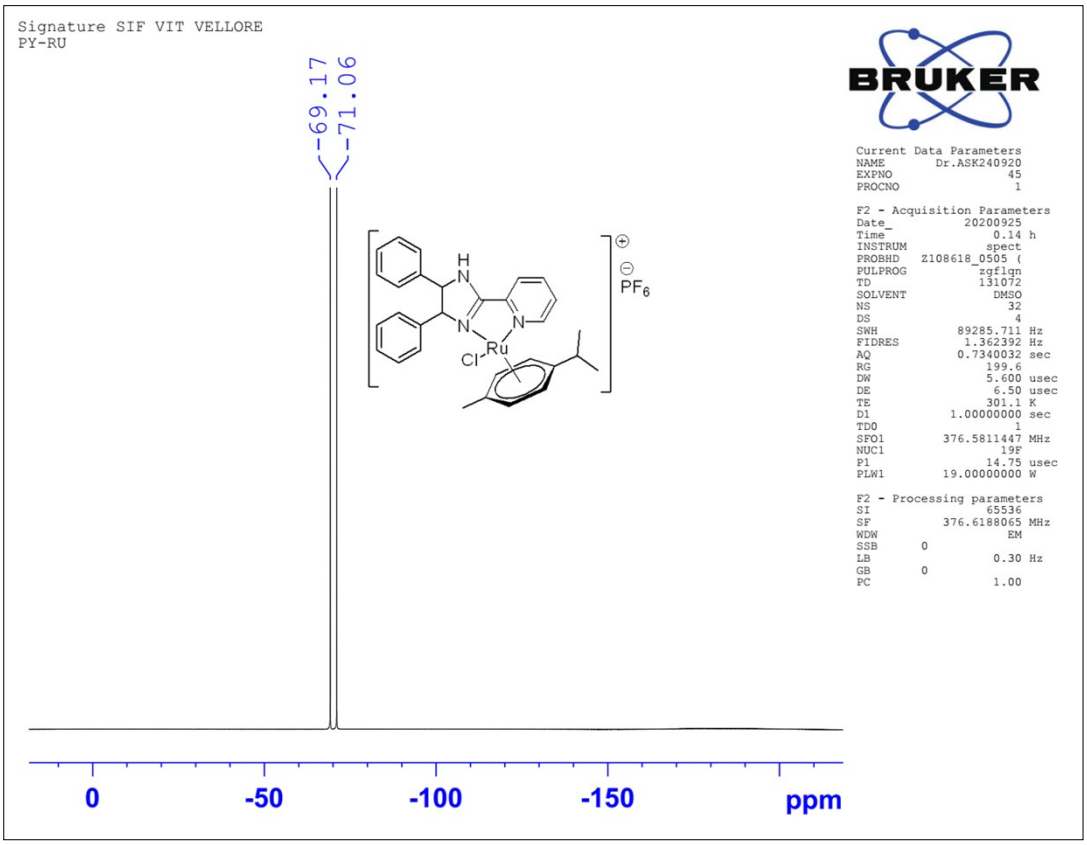

Fig. S12 ^{19}F NMR spectrum of **Ru-1**

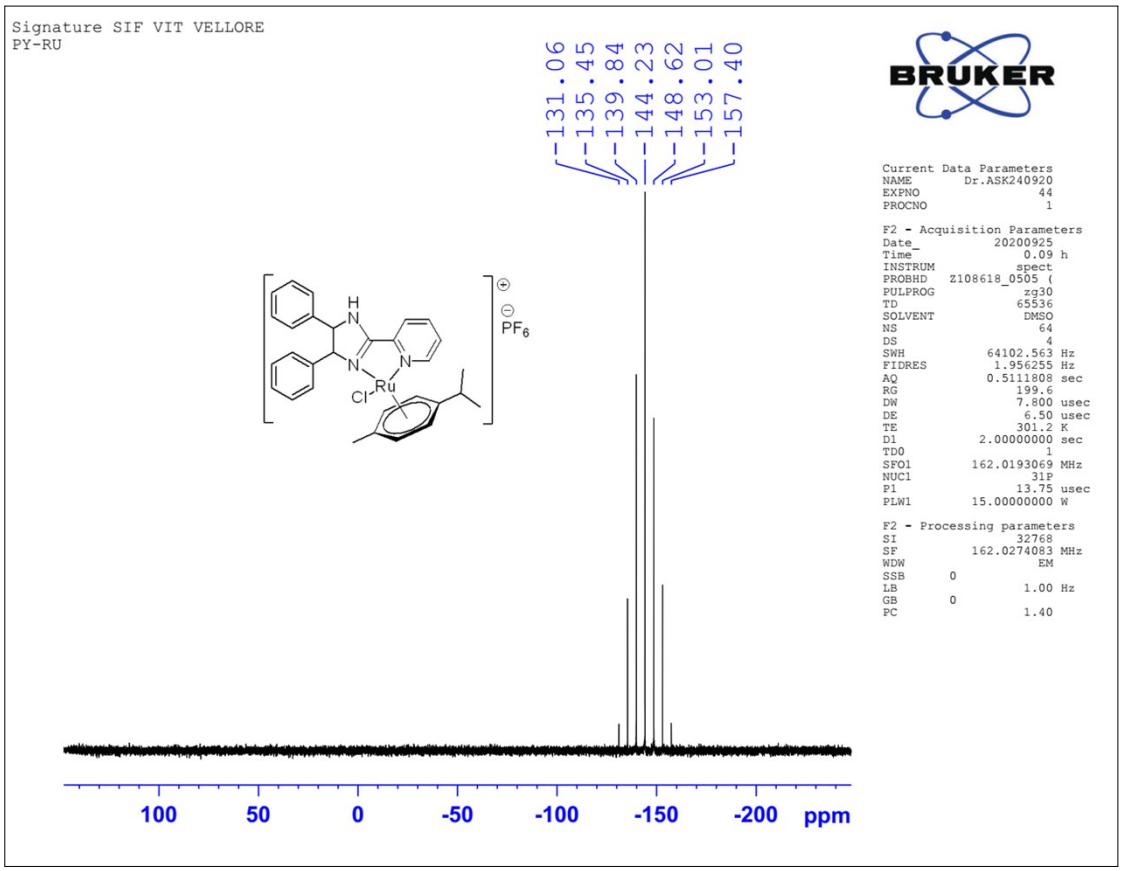

Fig. S13 ^{31}P NMR spectrum of **Ru-1**

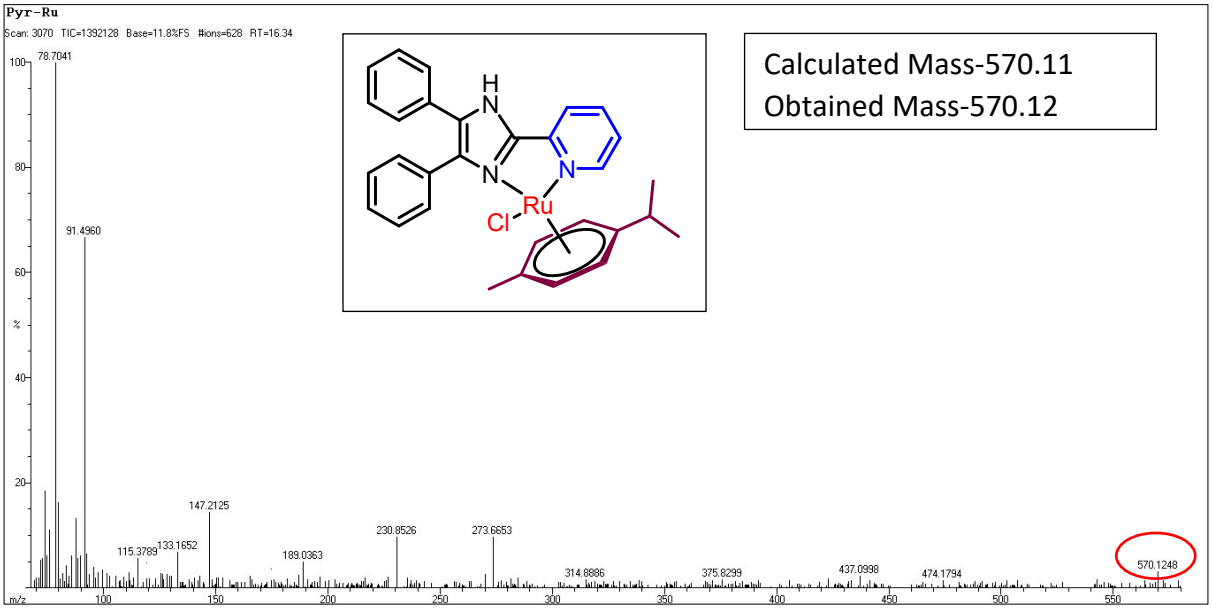

Fig. S14 HR-MS spectrum of **Ru-1**

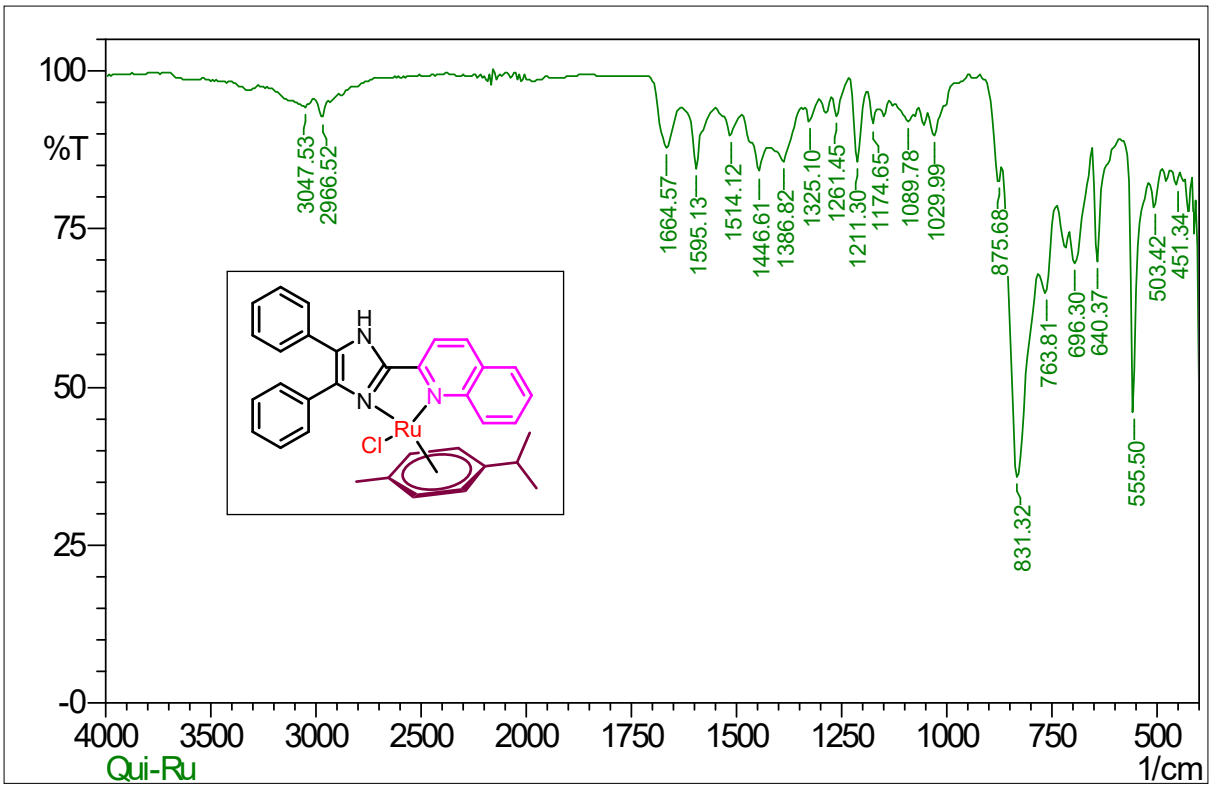

Fig. S15 FTIR spectrum of **Ru-2**

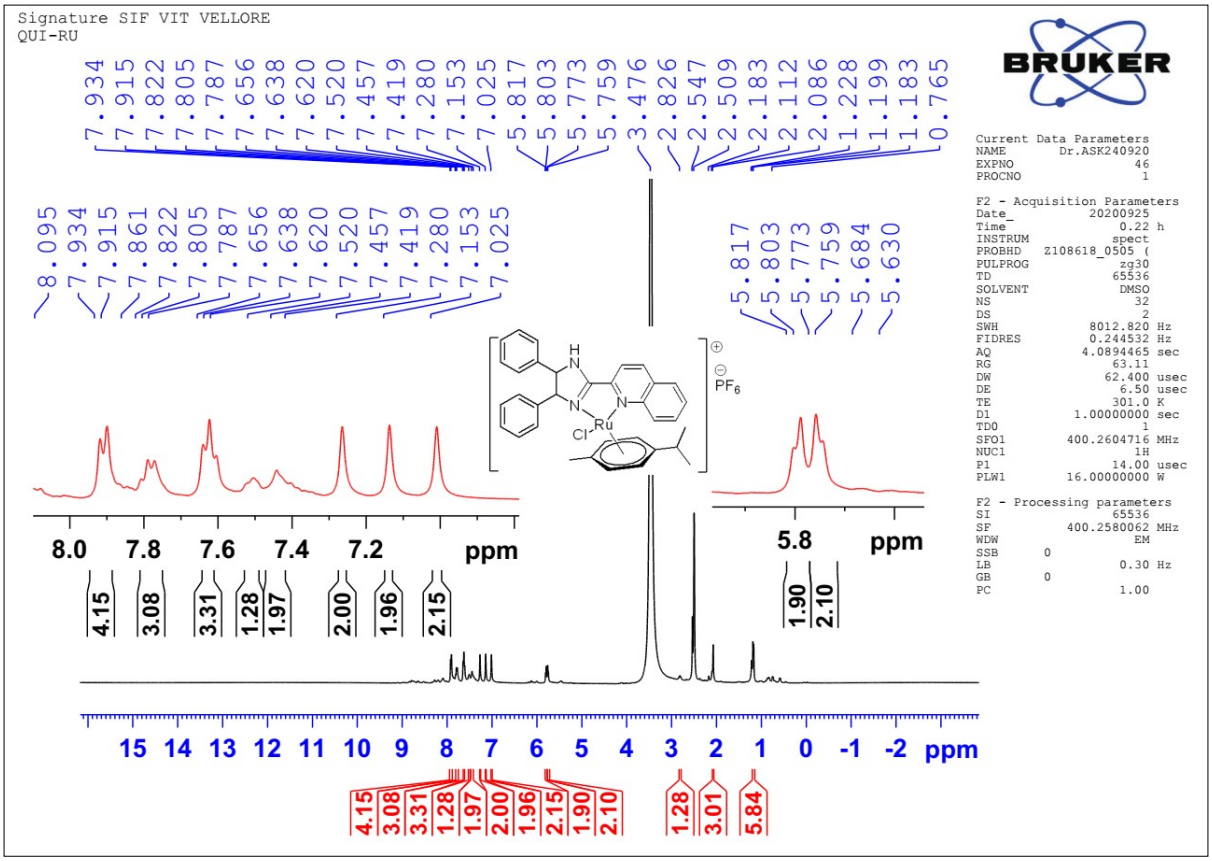

Fig. S16 ^{1}H NMR spectrum of **Ru-2**

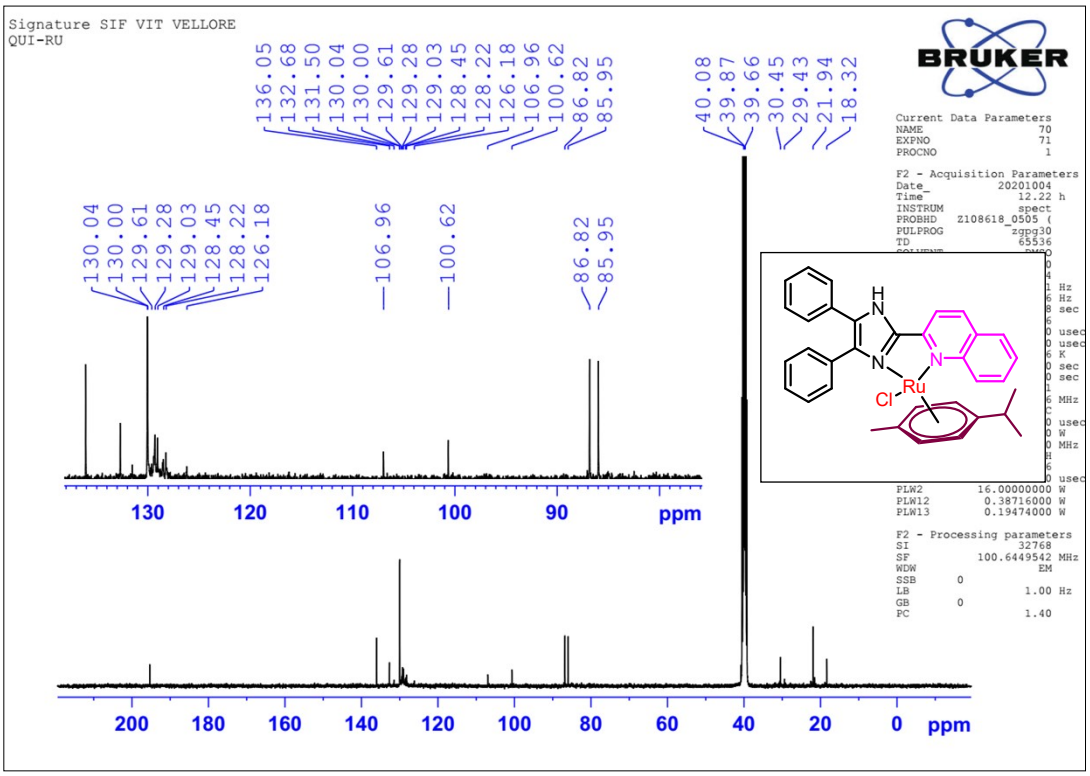

Fig. S17 ^{13}C NMR spectrum of **Ru-2**

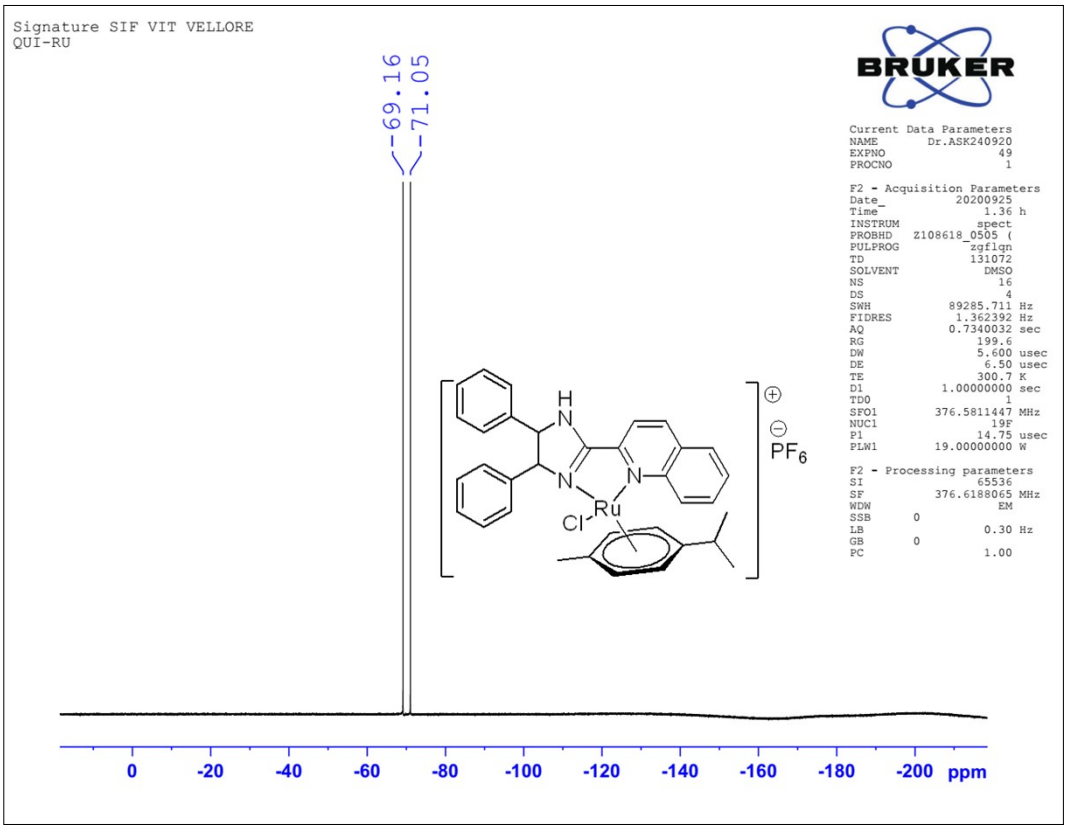

Fig. S18 ^{19}F NMR spectrum of **Ru-2**

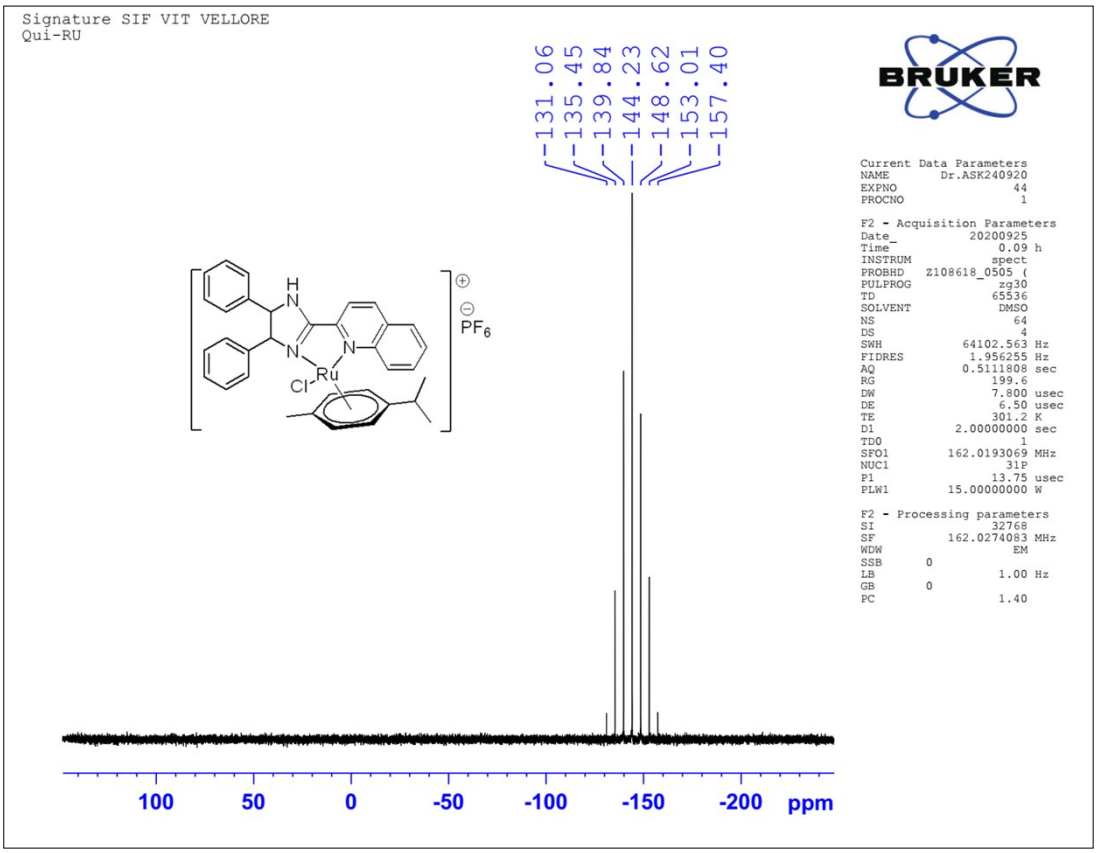

Fig. S19 ^{31}P NMR spectrum of **Ru-2**

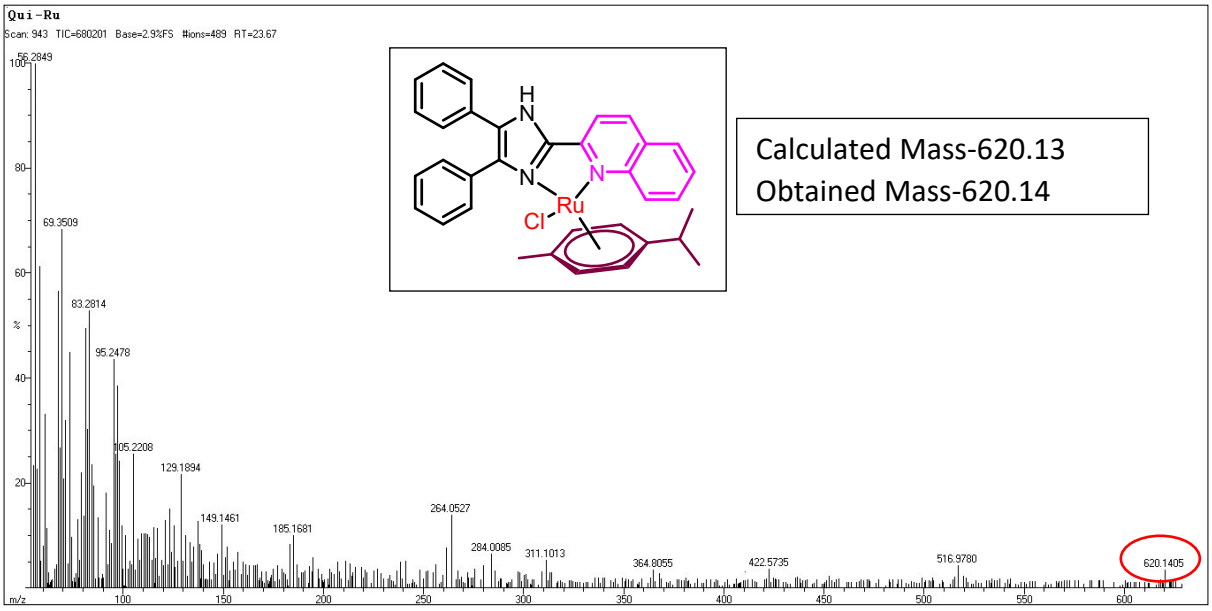

Fig. S20 HR-MS spectrum of **Ru-2**

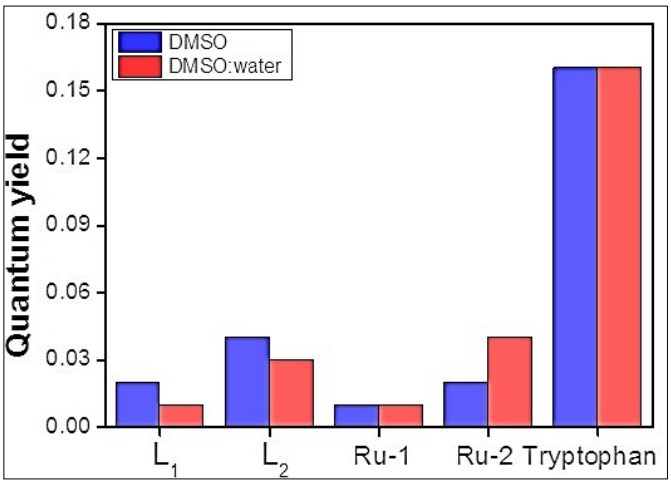

Fig. S21 Quantum yield of **L_1**, **L_2**, **Ru-1** and **Ru-2** in DMSO and DMSO: water condition

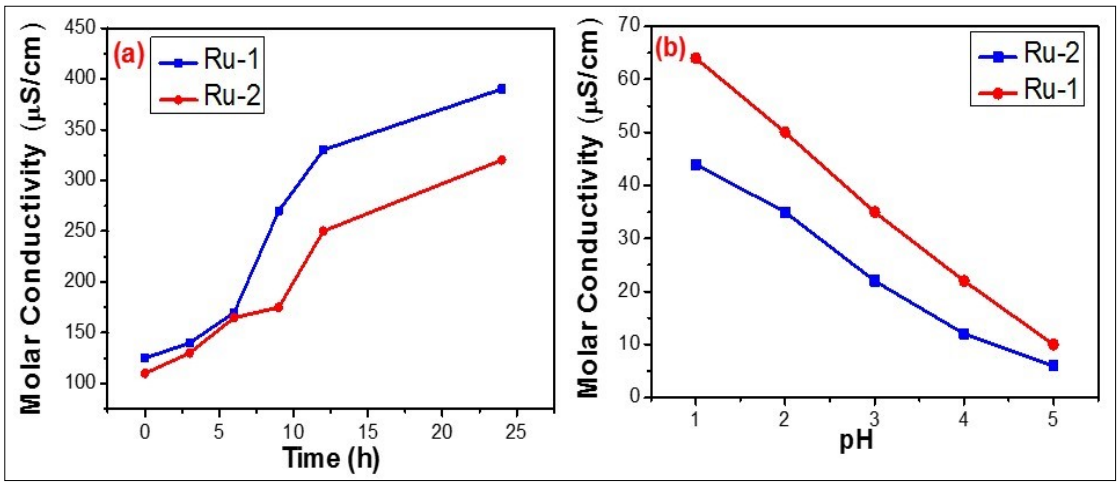

Fig. S22 (a) Time dependent molar conductivity (b) pH dependent molar conductivity

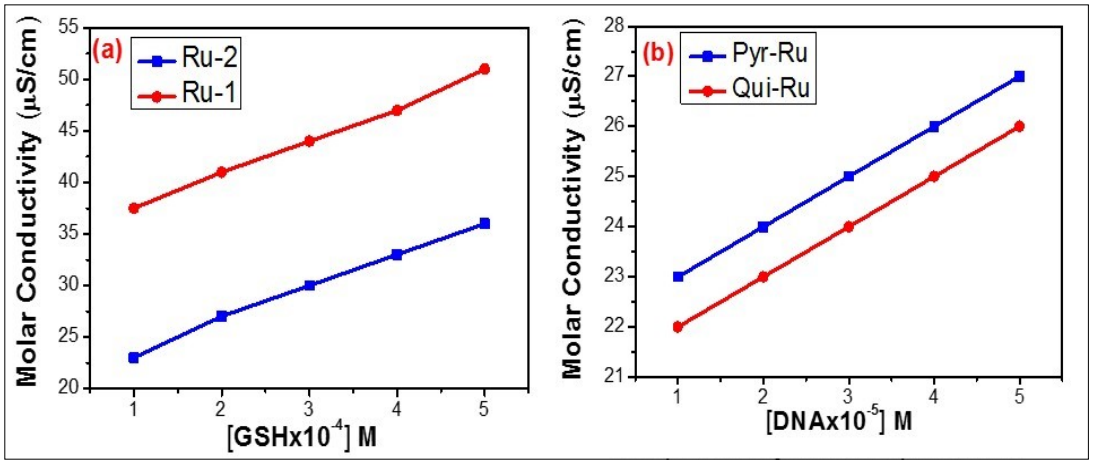

Fig. S23 (a) GSH dependent molar conductivity of compound in DMSO (b) Conductivity of compounds in DMSO with the increasing concentration of CT-DNA

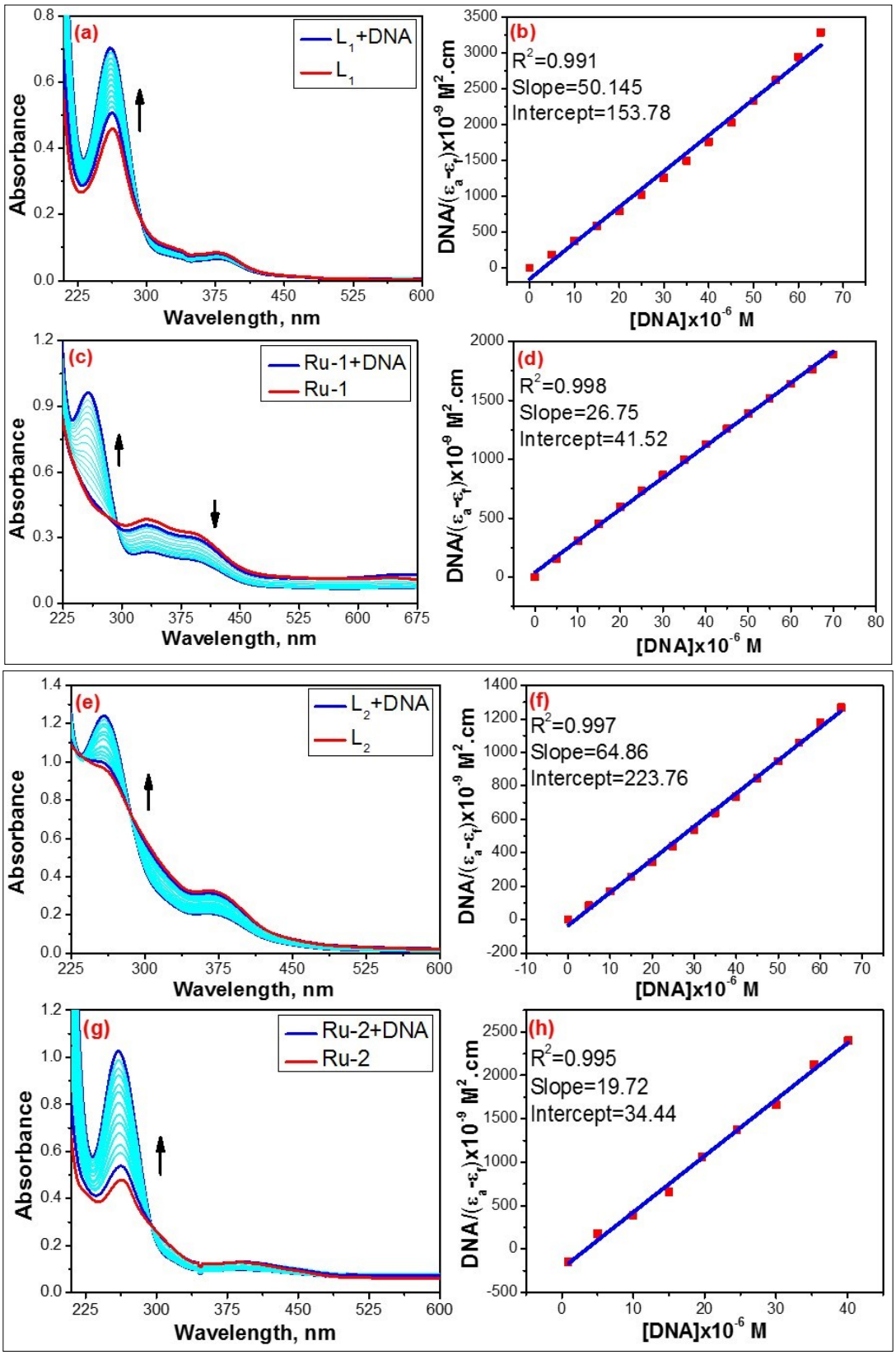

Fig. S24 Absorption spectral changes of (a) $\mathbf{L_1}$ (c) **Ru-1** (e) $\mathbf{L_2}$ and (g) **Ru-2** upon addition of DNA in 5 mM Tris-HCl-NaCl buffer The inset show the plot of [*DNA*]/($\varepsilon_a - \varepsilon_f$) versus [*DNA*] for the titration of the prepared compounds with CT–DNA.

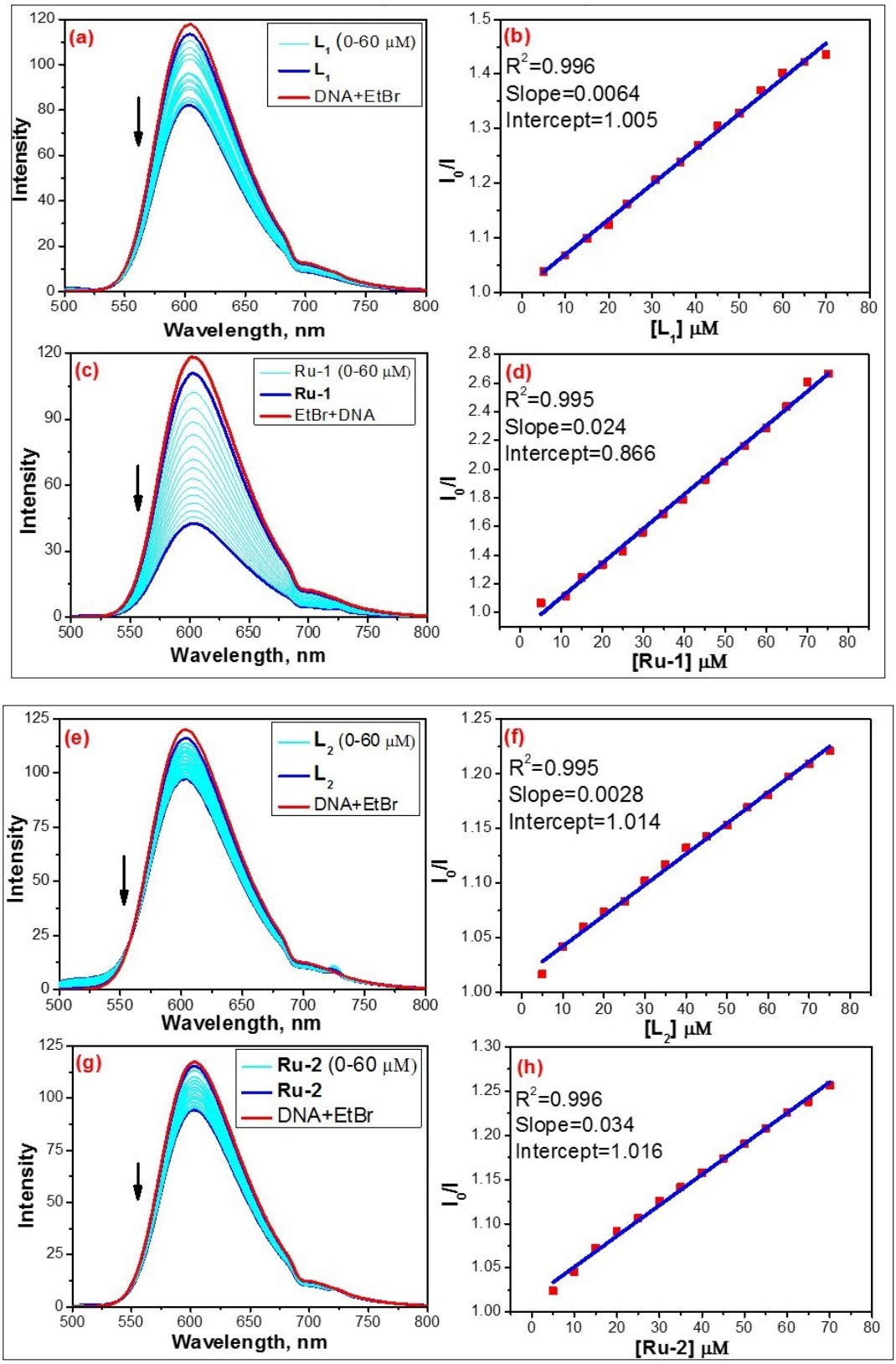

Fig. S25 Emission spectral changes on addition of lead compound (a) **L_1** (c) **Ru-1** (e) **L_2** and (g) **Ru-2** to CT-DNA bound to EtBr in 5 mM Tris-HCl /NaCl buffer of pH 7.2 and Stern-Volmer plot of I_0/I vs. compound (b) **L_1** (d) **Ru-1** (f) **L_2** and (h) **Ru-2** (λ_{ex}=485 nm and λ_{em}=590-598 nm)

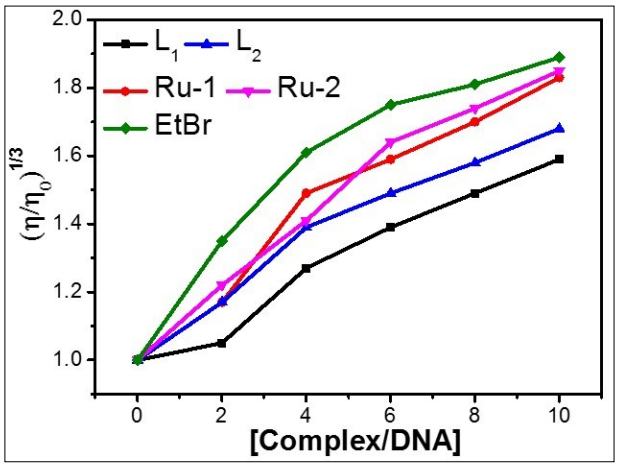

Fig. S26 Relative specific viscosities of CT-DNA in the presence of increasing amounts of the lead compounds and EtBr at 25°C in 5 mM Tris-HCl buffer at pH = 7.2.

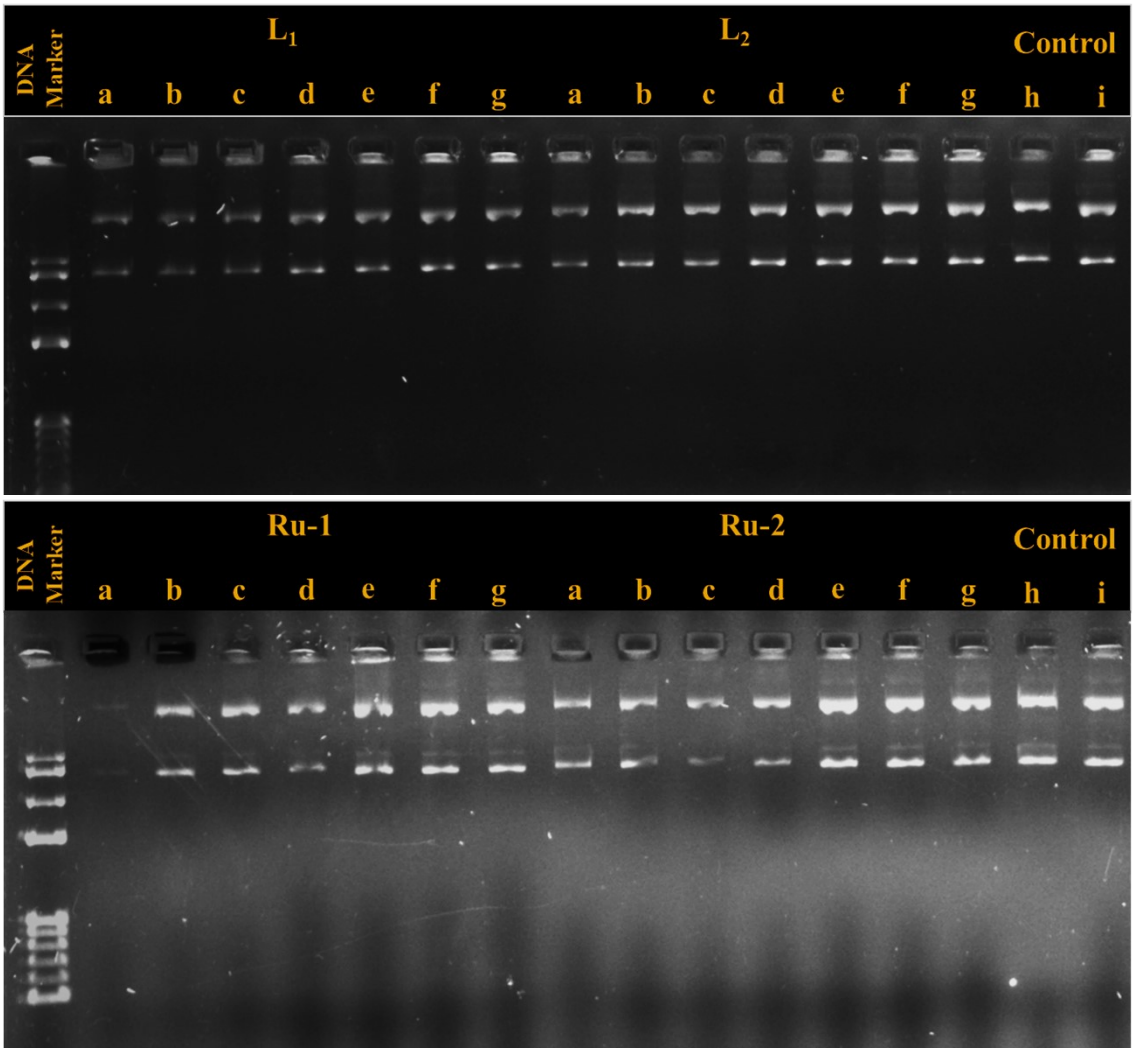

Fig. S27 Gel electrophoresis diagram showing chemical nuclease activity of **L_1**, **L_2**, **Ru-1** and **Ru-2**: (a) 1mM (b) 0.5 mM (c) 0.25mM (d) 0.125mM (e) 0.060 mM (f) 0.030 mM (g) 0.005mM (h) Control-DMSO +DNA (i) Control - PBS+DNA

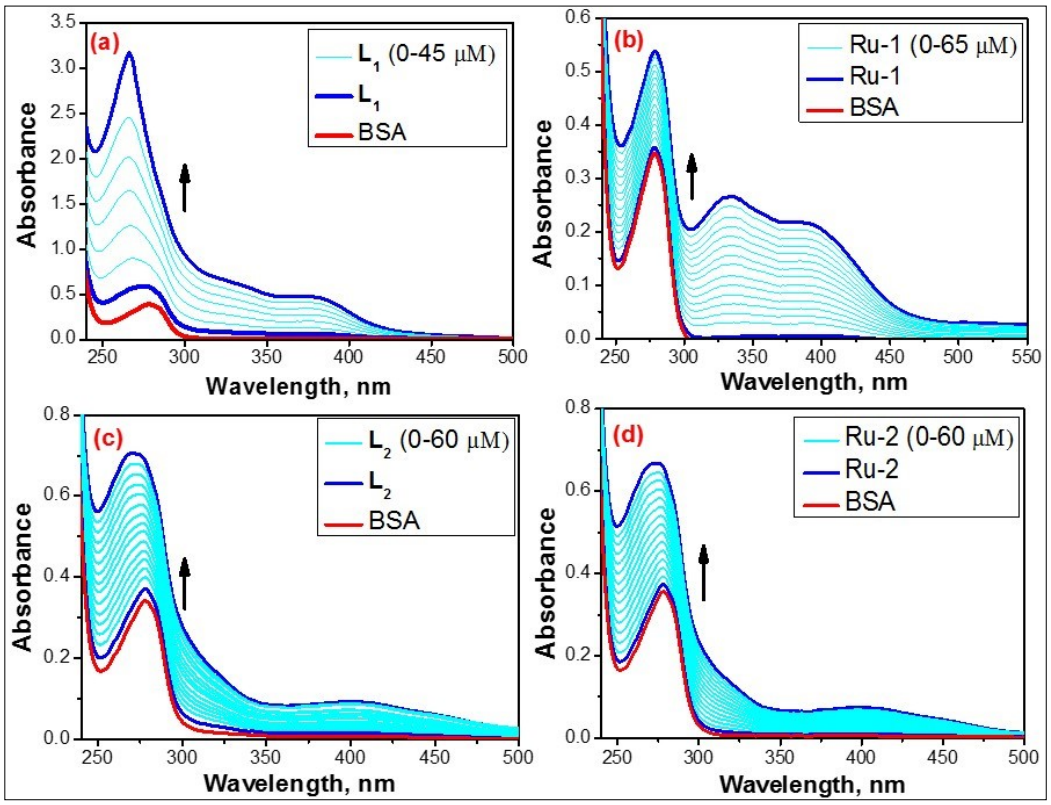

Fig. S28 Absorption spectral changes of BSA (3×10^{-5} M) in in 5 mM Tris-HCl/NaCl buffer at pH 7.2 upon increasing addition of (a) $\mathbf{L_1}$ (3×10^{-5} M) (b) **Ru-1** (c) $\mathbf{L_2}$ and (d) **Ru-2**

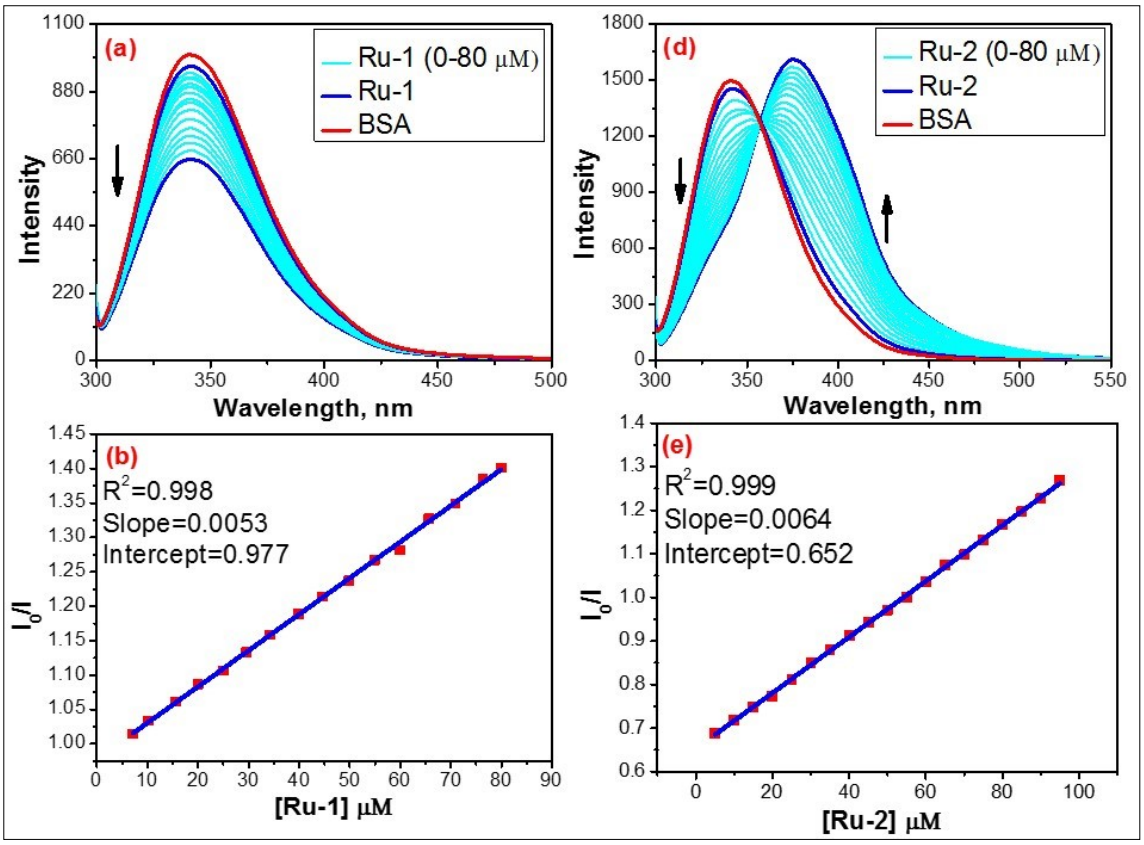

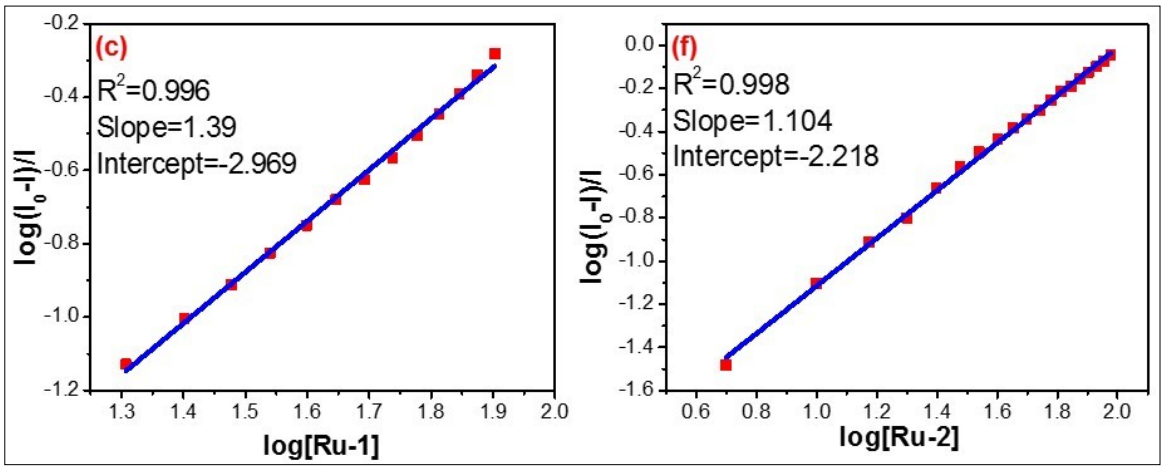

Fig. S29 Fluorescence quenching of BSA upon addition of compound (a) **Ru-1** and (d) **Ru-2** in 5 mM TrisHCl/NaCl buffer at pH 7.2 at 298 K (λ_{ex} = 295 nm). Plot of I_0/I vs. concentration of compounds (b) **Ru-1** and (e) **Ru-2**. Scatchard plot of $\log([I_0\text{-}I]/I)$ vs. log[complex] for BSA in the presence of compound (c) **Ru-1** and (f) **Ru-2**

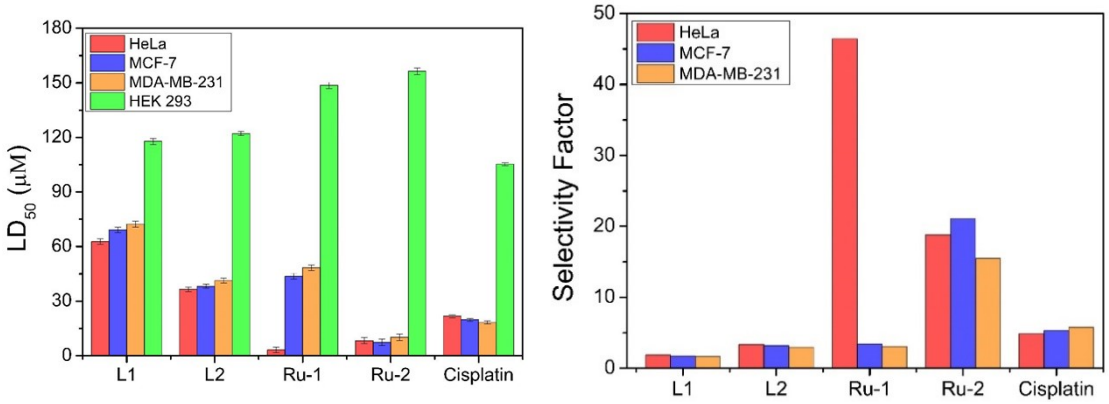

S30. Histogram illustrating the *In-vitro* Cytotoxicity assay of **L_1**, **Ru-1**, **L_2** and **Ru-2**

Table S1. Molecular docking studies of **L_1**, **L_2**, **Ru-1** and **Ru-2** with DNA and BSA

Ligand	Binding free energy ($\Delta G_{binding}$)$^{\alpha}$	Vdw_hb_desolv energy ($\Delta G_{vdW+hb+desolv}$)	Electrostatic energy (ΔG_{elec})	Total internal energy (ΔG_{total})	Torsional free energy (ΔG_{tor})	Unbound system's energy (ΔG_{unb})
DNA						
L_1	-7.7	-7.2	-0.91	-0.47	0.41	-0.47
L_2	-8.6	-8.2	-1.03	-0.58	0.62	-0.58
Ru-1	-8.0	-7.3	-1.11	-0.65	0.41	-0.65
Ru-2	-8.1	-7.4	-1.03	-0.63	0.33	-0.63
BSA						
L_1	-10.3	-9.6	-0.97	-0.54	0.27	-0.54
L_2	-10.6	-9.8	-1.01	-0.67	0.21	-0.67
Ru-1	-8.9	-8.3	-0.92	-0.53	0.32	-0.53
Ru-2	-8.7	-8.1	-1.07	-0.59	0.43	-0.59

Table S2. In silico prediction of physicochemical properties, toxicology, pharmacokinetics, drug-likeness of **L_1**, **L_2**, **Ru-1** and **Ru-2**

Properties/Ligand	L_1	L_2	Ru-1	Ru-2	Doxorubicin
Toxicology					
Toxic	No	Yes	No	No	No
Molecular Weight (gm/mol)	299.37	349.43	570.12	620.14	543.52
TPSA (A^2)	37.28	37.28	27.63	27.63	206.07
Hydrogen Donor	1	1	1	1	6
Hydrogen acceptor	2	2	1	1	12
Consensus Log P	3.31	4.3	4.7	5.45	1.17
Pharmacokinetics					
GI absorption	High	Low	High	High	Low
BBB permeant	Yes	No	No	No	No
Log Kp (skin permeation)	-4.91 cm/s	-6.34cm/s	-7.97 cm/s	-2.99 cm/S	-8.71 cm/s
P-gp substrate	Yes	Yes	Yes	Yes	Yes
CYP1A2 inhibitor	Yes	Yes	No	No	No
Drug-likeness					
Lipinski	Yes	1	2	2	No; 3 violations: MW>500, N or O>10, NH or OH>5
Ghose	Yes	Yes	Yes	No	No
Veber	No	No	No	No	No
Bioavailability Score	0.55	0.17	0.55	0.55	0.17

Table S3. Experimentally observed and TD-DFT calculated electronic transitions of L_1, L_2, Ru-1 and Ru-2.

Lead compounds	Experimental		Theoretical			
	λ_{max} (nm)	ε (L. M^{-1}.cm^{-1})	λ_{max} (nm)	Oscillator strength (f)	Transition	Orbital Contribution
L_1	264	1.4×10^4	259.89	0.1477	$S_0 \rightarrow S_7$	75% H-2 → L & 6.8% H → L+5
			337.9	0.4514	$S_0 \rightarrow S_1$	98.6% H → L
L_2	261	4.1×10^4	250.17	0.3679	$S_0 \rightarrow S_{14}$	36.86 % H-1 → L+1, 15.63% H → L+4 & 12.73% of H-6 → L
			327.45	0.2638	$S_0 \rightarrow S_2$	95% H → L+1
Ru-1	331	5.3×10^3	300.76	0.0626	$S_0 \rightarrow S_{28}$	33.95% H-2 → L+4, 26.37% H-4 → L+1 & 18.82% H-1 → L+4
			398.23	0.0858	$S_0 \rightarrow S_8$	55% H-2 → L, 14.63% H-1 → L & 8.14% H-3 → L
Ru-2	263	7.0×10^3	289.92	0.196	$S_0 \rightarrow S_{28}$	48.57% H-1 → L+3 & 7.70% H-1 → L+3
			391.34	0.1575	$S_0 \rightarrow S_8$	25.41% H-1 → L+1, 19.72% H-2 → L+3 & 16.57% H-3 → L

*H – HOMO, L – LUMO orbitals

References

1. M. Shamsi-Sani, F. Shirini, M. Abedini, M. Seddighi, *Res. Chem. Intermed*. 2016, **42**, 1091–1099.
2. I. Ali, W. A. Wani, K. Saleem, *Synthesis and Reactivity in Inorganic, Metal-Organic, and Nano-Metal Chemistry*. 2013, **43**, 1162-1170.
3. M. Sirajuddin, S. Ali, A. Badshah, *J. Photochem. Photobiol., B*. 2013, **124**, 1–19.
4. M. V. Bharathi, S. De, T. Lavanya, S. Maiti, B. Sarkar, S. K. Ashok Kumar, and P. Paira. *New J. Chem*, 2018, **42**, 9116-9125.
5. S. De, B. Sarkar, G.R. Jadhav, S.K. Ramasamy, S. Banerjee, A. Moorthy, P. Paira, S.K. Ashok Kumar, *ChemistrySelect*. 2018, **3**, 10593–10602.
6. S. Banerjee, I. Pant, I. Khan, P. Prasad, A. Hussain, P. Kondaiah, A.R. Chakravarty, *Dalton Trans*. 2015, **44**, 4108–4122.
7. J. H. Shi, J. Chen, J. Wang, Y. Y. Zhu, *Spectrochim. Acta, Part A*, 2015, **136**, 443–450.
8. R. K. Vuradi, K. Dandu, P. K. Yata, R. R. Mallepally, N. Chintakuntla, R. Ch, S.S. Thakur, C.M. Rao, S. Satyanarayana, *New J. Chem*. 2018, **42**, 846–859.
9. S. Dasari, A. K. Patra, *Dalton Trans*. 2015, **44**, 19844–19855.
10. J. Keizer, *J. Am. Chem. Soc*. 1983, **105**, 1494–1498.
11. R.G. Pearson, *J. Org. Chem*. 1989, **54**, 1423–1430

12. V. D. Suryawanshi, L. S. Walekar, A. H. Gore, P. V. Anbhule, G. B. Kolekar, *J. Pharm. Anal*. 2016, **6**, 56–63.
13. K. Singh, P. Srivastava, A.K. Patra, *Inorg. Chim. Acta*, 2016, **451**, 73-81
14. J. Liu, J. Tian, W. He, J. Xie, Z. Hu, X. Chen, *J. Pharm. Biomed. Anal*. 2004, **35**, 671–677.
15. H. Y. Lu, S. H. Yang, J. Deng, Z. H. Zhang, *Aust. J. Chem*. 2010, **63**, 1290–1296.
16. S. De, S.K. Ashok Kumar, *Inorg. Chem. Commun*. 2020, **119**, 108085.
17. M. Kubanik, H. Holtkamp, T. Söhnel, S. M. F. Jamieson, and C. G. Hartinger, *Organometallics*, 2015, **34**, 5658–5668.
18. H. Cumming, C. Rucker, *ACS Omega*, 2017, **2**, 6244–6249.
19. S. De, S. Banerjee, S.K. Ashok Kumar, P. Paira, *Mini-Rev. Med. Chem*. 2019, **19**, 88-97.
20. M. Kubanik, H. Holtkamp, T. Söhnel, S. M. F. Jamieson and C. G. Hartinger, *Organometallics*, 2015, **34**, 5658–5668.
21. O. Trott, A. J. Olson, *J. Comput. Chem*. 2010, **31**, 455–461.
22. A. Chandra, K. Singh, S. Singh, S. Sivakumar, A. K. Patra, *Dalton Trans*. 2016, **45**, 494–497
23. H. Rozenberg, D. Rabinovich, F. Frolow, R.S. Hegde, Z. Shakked, *Proc. Natl. Acad. Sci*. 1998, **95**, 15194–15199.
24. P. W. Rose, A. Prlic, C. Bi, W. F. Bluhm, C. H. Christie, S. Dutta, R. K. Green, D.S. Goodsell, J. D. Westbrook, J. Woo, *Nucleic Acids Res*. 2014, **43**, D345–D356.
25. N. M. O'Boyle, M. Banck, C. A. James, C. Morley, T. Vandermeersch, G. R. Hutchison, *J. Cheminf*. 2011, **33**, 1–14.
26. A. Bujacz, *Acta Crystallogr Sect. D: Biol. Crystallogr*. 2012, **68**, 1278–1289.
27. G. Sudlow, D. J. Birkett, D. N. Wade, *Mol. Pharmacol*. 1976, **12**, 1052–1061.
28. E. Scrocco, J. Tomasi, in L. Per-Olov (Ed.), *Academic Press*, 1978, 115–193.
29. M. Govindarajan, S. Periandy, K. Carthigayen, *Spectrochim. Acta Part A: Mol. Biomol. Spectrosc*. 2012, **97**, 411–422